

# Section B

## Joint Research

# Highlights of Joint Research

## Synchrotron Radiation Laboratory

Synchrotron Radiation Laboratory (SRL) has been promoting the project for constructing a new synchrotron radiation facility dedicated to the science in VUV (or EUV) and Soft X-ray (SX) region, which has been discussed at the Panel on New Synchrotron Radiation Facility Project. The new light source consists of a 1.8 GeV electron storage ring and the injector system. The normal cell lattice of the storage ring is a DBA type with twelve 6.2-m normal length straight sections, two of which will be used for the injection part and the RF cavity installation, and two 17-m long straight sections. The injector consists of a 200 MeV lineac and a 2.0 GeV booster synchrotron. The conspicuous feature of the new light source is that every part of the accelerators is designed adapting to the "top-up injection" to overcome the short lifetime of the electron beam in a storage ring operated with relatively low energy.

The details of the new facility have been discussed and planned with nationwide supports by accelerator scientists and engineers as well as researchers using synchrotron radiation. The results of the discussion are summarized as a "New Synchrotron Radiation Project -Design Report-" (in Japanese) in September 2002. The University of Tokyo strongly endorsed the project to construct the proposed new facility in the Kashiwa campus. The plan is supported not only by researchers in academic institutions but also bio and chemical-industries. The figure below shows an image of the new facility as constructed in the Kashiwa campus.

The staff members of SRL have been continuing the research and developments of the light source, beamlines and monochromators. The accelerator group of SRL is carrying out research works of the accelerator physics and developing the accelerator-related technology, many of which will be directly applied to the new light source. The research highlight of 2002 is electron-beam size measurement with a newly developed beam profile monitor. The monitor is a real-time and non-destructive monitor with a high spatial resolution and has a microscopic structure, where two Fresnel zone plates constitute an X-ray imaging optics. With this monitor, our group has succeeded in obtaining a clear electron-beam image and measuring the electron-beam size less than 10  $\mu\text{m}$  in the KEK-ATF damping ring.

On the other hand, the branch laboratory at KEK-Photon



Factory maintains an undulator called Revolver, two beamlines and three experimental stations for angle-resolved photoelectron spectroscopy (ARPES), spin- and angle-resolved photoelectron spectroscopy (SARPES) and soft X-ray emission spectroscopy (XES), which are fully opened to outside users. The SRL staffs not only serve the outside users with technical support and advices, but also carry out their own research works on advanced solid state spectroscopy as well as instrumentation. In the fiscal year of 2002, the operation time of the beamlines was more than 5000 hours and the number of the users was more than 200.

The scientific highlights of the beamlines achieved in 2002 are found in the studies of the electronic structures of a ferroelectric  $\text{Bi}_4\text{Ti}_3\text{O}_{12}$  observed by XES, of an alkaline-metal doped  $\text{C}_{60}$  adsorbed on Si surfaces studied by ARPES. The SARPES experiments on Co/Pd(111) shows that the re-orientation of the magnetization direction observed in Co films is the result of the increase of Co 3d electrons with orbital moment parallel to the surface as the Co film thickness increases.

## Neutron Scattering Laboratory

Since 1961, the ISSP has been playing a central role in neutron scattering activities in Japan not only by performing its own research programs but also by providing a general user program for the university-owned various neutron scattering spectrometers installed at research reactors of JAERI (Tokai). By spending 5 years starting from 1988, the ISSP constructed total 8.5 highly-sophisticated spectrometers both in a reactor hall and in a guide hall of the refurbished JRR-3M reactor (20 MW) with cold source. In addition, Tohoku University owns 3.5 spectrometers and Kyoto University 1; therefore, total 13 spectrometers belong to the university while JAERI owns 9. In order to fully utilize these facilities, the previous Neutron Scattering Division of ISSP at Tokyo was promoted to the present Neutron Scattering Laboratory at Tokai in 1993. Since then, close to 300 proposals are submitted for the ISSP general user program for neutron scattering research each year, and the number of visiting users under this program reaches over 7000 (person-day/year). Major research areas are solid state physics (strongly correlated electron systems, high  $T_c$  superconductors, heavy fermion systems, low dimensional magnetism, high-pressure physics etc.), fundamental physics and neutron beam optics, polymer, chemistry, biology, and materials sciences.

Triple axis spectrometers and a high resolution powder diffractometer were utilized for a conventional solid state physics and a variety of research fields on hard-condensed matter, while in the field of soft-condensed matter physics, researches were mostly carried out by using the small angle neutron scattering (SANS-U) and/or neutron spin echo (NSE) instruments. In the fiscal year of 2002, the research topics on the hard-condensed matter science covered stripe order in high- $T_c$  superconductors, and closely related 2 dimensional systems, charge and orbital ordering in CMR manganites, quadrupolar ordering in rare-earth based intermetallic compounds, spin dynamics of low dimensional dimer systems, etc. On the other hand, the research topics on the soft-condensed matter science covered structure char-

acterization of polymer blends, micelles, amphiphilic polymers block copolymers, liquid crystals, proteins, inorganic gels, dynamics of brush-polymers on surface, slow dynamics of surfactants, pressure dependence of dynamics of amphiphilic membranes, and so on. The details of individual studies are reported in the NSL-ISSP Activity Report 2003 (vol.10).

## Supercomputer Center

The supercomputer system in the Supercomputer Center of the Institute (SCC-ISSP) is placed at the service of general researchers of condensed matter physics through the User Program conducted by the Materials Design and Characterization Laboratory (MDCL). One of its aims is to selectively promote and support huge computations which are hardly carried out on other computers such as work-station clusters in individual laboratories.

The SCC-ISSP main system consists of two supercomputers. Hitachi SR8000/60, called System-A, is a distributed-memory-type parallel supercomputer with 60 nodes, 640 GB memory in total and  $12 \times 60$  GFlops peak performance. On the other hand, SGI Origin 2800/384, called System-B, is a massively parallel supercomputer with 192 GB memory in total and  $0.8 \times 384$  GFlops peak performance.

A project(s) can be proposed by any staff in universities or public research institutes in Japan. The projects proposed are judged by the Steering Committee of the SCC-ISSP, under which the Supercomputer Project Advisory Committee is formed to review proposals. More than half of the members of each committee are those in other institutions than the ISSP. The number of projects, the total points applied and approved in this year are listed on Table. 1

The research projects carried out on the system cover various fields in the condensed matter physics. They are roughly classified into the following three (the number of projects approved):

- First-Principles Calculation of Materials Properties (52)
- Strongly Correlated Quantum Systems (60)
- Cooperative Phenomena in Complex, Macroscopic

Systems (22)

All the three involve both methodology of computation and its applications. The results of all the projects are reported in ‘Activity Report 2002’ of the SCC-ISSP. In the report the following five invited articles are included in this year:

- “Equilibrium and off-equilibrium simulations of the three-dimensional Heisenberg spin glass (S-class project)” by Hikaru Kawamura and Koji Hukushima,
- “First-principles study with Diffusion Monte Carlo code” by Ryo Maezono,
- “Theoretical Analyses of Electric-Current Related Phenomena at Surface Nanostructures under Strong Local Electric Field” by Satoshi Watanabe, Yoshihiro Gohda, Shinnosuke Furuya, Noriko Tanaka, Chunping Hu and Hideomi Totsuka,
- “Monte Carlo study of ferromagnetic transition in double-exchange” by Yukitoshi Motome and Nobuo Furukawa,
- “Large Spins and High-Order Interactions” by Naoki Kawashima and Kenji Harada.

Based on the discussions at the ISSP Workshop “Computational Physics for Condensed Matter Research” held in November 2002, the home page

<http://www.issp.u-tokyo.ac.jp/public/cmp>

and the mailing list ‘cmp-ml’ were set up for communicating information not only on the SCC-ISSP but on general research activities in the field of ‘Computational Material Physics’.

Table 1: Research projects approved in 2002

Class	Max. Point	Application	# of Proj.	Total points			
				Applied		Approved	
				Sys-A	Sys-B	Sys-A	Sys-B
A	100k	any time	3	210K	90K	210K	90K
B	2M	twice a year	48	63.5M	27.35M	61.5M	27.05M
C	20M	twice a year	72	763.5M	375.0M	696.2M	351.0M
D	none	any time	11	125.0M	269.0M	40.0M	197.0M

For System-A 1 K point corresponds to charge for CPU time of about 0.43 hours by one processing element, while the corresponding figure is 2.32 hours for System-B. For one of the D class projects, a special queue which exclusively uses 2 nodes of system-A was allowed to perform extremely long-time jobs necessary.

# High Resolution Atomic Force Microscopy by Detection of a Single Chemical Bonding

T. Eguchi, Y. Hasegawa and T. Sakurai

Atomic force microscopy (AFM) provides surface images of various materials regardless to its electrical conductance by detecting a force acting between the sample surface and probe tip. Recent developments for a force detection technique make us possible to take images with nanometer-scale spatial resolution. Compared with scanning tunneling microscopy (STM), however, its spatial resolution has been still limited. One of the reasons for the limited resolution is a significantly large site-insensitive background component due to the van der Waals (vdW) force. In this study we succeeded in achieving highly resolved AFM imaging by reducing the background force and detecting a force arising from a single chemical covalent bonding by using small oscillation amplitude of the cantilever and an atomically sharp tip [1]. Since the chemical bonding is in nature a short range force, it works as a extremely sensitive probe, similar with the tunneling current of STM.

Figure 1 shows a typical AFM image taken in this study. In the image, individual adatoms of the dimer-adatom-stacking fault (DAS) structure are clearly imaged. In addition, hump features are obviously observed at the sites exactly corresponding to the rest-atoms. In the area where adatom is missing, the second-layer atoms are also clearly resolved.

In order to analyze what kinds of forces are working between the sample and probe tip, we measured the force as a function of the tip-sample distance (i.e. force curve). Such a force profile is shown in Fig. 2. When the tip and sample are separated more than 1 nm, the force varies gradually, and at the proximate distances below 1 nm, the force changes steeply. The gradually-varied force is due to the long-range vdW force, and the steep one is due to a chemical covalent

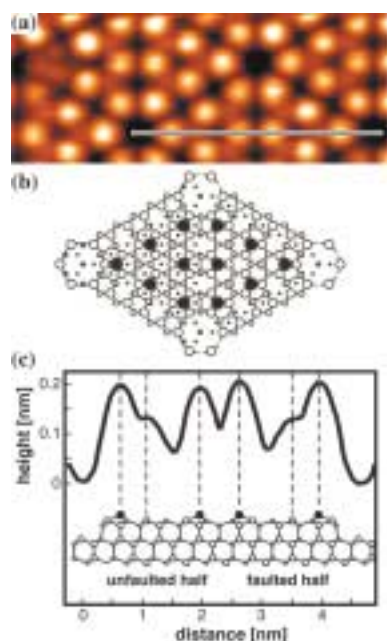


Fig. 1. (a) An atomically resolved AFM image of the Si(111)7x7 surface. The observed area of the AFM image is 7.5 nm x 3.0 nm. (b) Top view of the DAS structural model of the Si(111)7x7 surface. (c) A cross-sectional plot measured on the long diagonal line of the 7x7 unit cell drawn in (b), together with a side view of the DAS structural model, demonstrating a precise fitting of adatom and rest-atom positions.

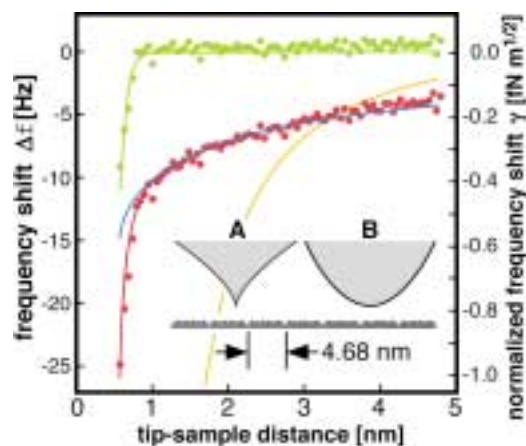


Fig. 2. A frequency shift versus tip-sample distance curve (force curve) measured on the Si(111)-(7x7) surface. Experimental data points are marked with a red filled circle. The fitted line is drawn with a red line. A blue line depicts a component by the long-range vdW force, and a green circle shows the experimental data points minus the component of the long-range force. The green line is a component due to the short-range chemical force. The sum of the blue line and green line should be equal to the red fitted line. Inset: Model tip shape deduced from the fitting depicted with a side view of the surface structural model. Model A is fitted nicely with our experimental data and model B, a parabolic shape with an apex radius of 4 nm, is the one used for fitting in other works. A simulated long-range force curve with tip B is drawn in the plot (orange line), demonstrating a strong reduction of the background using tip A.

bonding between the atoms of the sample surface and Si tip apex. From a fitting with known parameters for the Si-Si bonding, it is found that the chemical bonding is due to a single bonding.

Since the total vdW force is a sum of vdW working on individual atoms composing the sample and tip, the shape of the tip can be deduced from the force profile, and found to be like tip A shown in an inset of Fig. 2. It should be noted that the tip apex is very sharp. As a comparison a force profile for a blunt tip (tip B) is calculated and plotted with an orange curve in Fig. 2. Obviously, with tip B the vdW force is large, dominating over the chemical force. It is thus difficult to obtain highly resolved images with tip B.

This study implies that characterization of the AFM tip in nanometer scale, not only on the apex atoms but also its shape near the apex, is important and critical for AFM high resolution imaging.

## Reference

[1] T. Eguchi and Y. Hasegawa, Phys. Rev. Lett., **89**, 266105 (2002).

## Authors

T. Eguchi, Y. Hasegawa, and T. Sakurai<sup>a</sup>

<sup>a</sup>Institute for Materials Research, Tohoku University

## LEED and STM Study of GaP(111)B Reconstructed Surface

K. Hattori and F. Komori

Gallium phosphide is one of the fundamental III-V compound semiconductors for optoelectronic devices. Various works on GaP crystals coupled with other materials have been performed to educe valuable functions of these systems. We have studied GaP(111)B (i.e., (-1-1-1), phosphorus face) reconstructed clean surface with low-energy electron diffraction (LEED) and scanning tunneling microscopy (STM). This surface is important because it has been used for the transparent substrate of GaAlAs diodes and for the

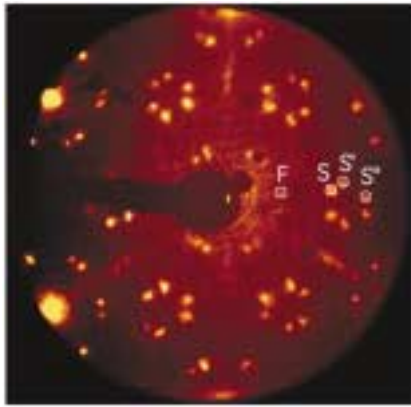


Fig. 1. A typical LEED pattern of GaP(111)B reconstructed surface at 30 eV. The pattern includes many super-spots (e.g., F, S, S' and S'') arising from the surface reconstruction.

buffer layer of well-growth InN film with an excellent electronic transport property, for instance.

The reconstructed LEED pattern of GaP(111)B surface is very complex. Figure 1 shows a typical pattern at 30 eV. So far, there have been two different explanations for the reconstructed unit with the assumption of a single domain formation on this surface; Bommel and Crombeen reported  $17 \times 17$  reconstruction [1], while Wang *et al.* suggested  $\sqrt{247} \times \sqrt{247}$ -R22.7° [2]. However, we found using STM that the reconstructed surface consists of six domains with stripe pattern. Figure 2(a) shows an STM image of the multiple domain area. The stripe directions are tilted from three  $\langle -1-12 \rangle$  (i.e.  $[-1-12]$ ,  $[-12-1]$  and  $[2-1-1]$ ) directions at  $6.8^\circ$ , and the stripe period is 1.30 nm. Therefore, the surface consists of six equivalent mirror-symmetric domains (three pairs of twin domains, A and B, C and D, and E and F).

A magnified STM image of the stripe structure is shown in Fig. 2(b). The reconstructed surface unit can be recognized by analyzing the arrangement of the atomic protrusions. On this surface, surprisingly, we found that two different unit cells exist; the same unit is repeated along the stripe but either the same or the different unit (with almost the same possibility) is arranged for the inter stripe direction.

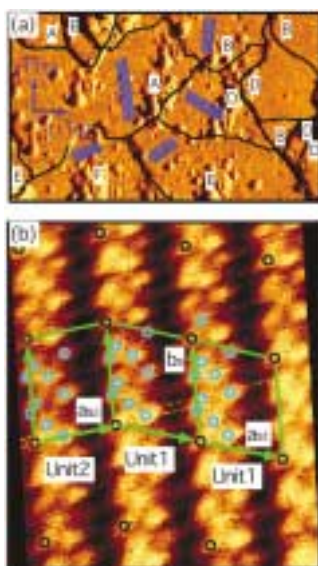


Fig. 2. STM images of GaP(111)B reconstructed surface, (a) 150 nm $\times$ 90 nm area showing multiple domains with stripe patterns (some with lines for the eye guide), and (b) 5.4 nm $\times$ 6.3 nm area the magnification of the stripe pattern. In Fig. (b) the black circles present the origins of surface reconstruction units, and each unit includes several protrusions. We can recognize the co-existence of the two different units.

The reciprocal lattice of the surface model with the random mixture of the two reconstructed units,  $((3 -1), (2 5))$  and  $((4 1), (2 5))$ , well explains the obtained LEED patterns (e.g., Fig.1) assuming the same elements positioned at the STM protrusions. Further analysis such as LEED I-V measurement will solve the atomic structure of the reconstructed GaP(111)B surface, based on these results.

#### References

- [1] A.J. Van Bommel and J.E. Crombeen, Surf. Sci. **93**, 383 (1980).
- [2] X. Wang, X.Y. Hou, X.M. Ding, G.S. Dong, X.K. Lu, and P. Chen, in "Surface Physics and Related Topics: Festschrift for Xide Xie", edited by F.-J. Yang *et al.*, (World Scientific Publishing, Singapore, 1991), p. 326.

#### Authors

K. Hattori<sup>a</sup>, K. Ishihara<sup>a</sup>, Y. Miyatake<sup>a</sup> and F. Komori<sup>a</sup>  
<sup>a</sup>Graduate School of Materials Science, Nara Institute of Science and Technology

## Charge Transfer at Oxide Interfaces

H. Kumigashira and M. Lippmaa

Oxide surfaces and interfaces often behave quite differently from bulk crystals. This can be seen easily in thin layers of  $\text{La}_{0.6}\text{Sr}_{0.4}\text{MnO}_3$  grown on various oxide surfaces. Although the bulk material is a ferromagnetic metal below about 300 K, single unit cell layers are usually insulating. Such a dramatic change in transport properties is caused by a charge transfer between the film and the underlying layer, effectively altering the carrier concentration in the thin film. Such changes have a large impact on the properties of oxide superlattices and heterostructures.

Our aim is to understand how the electronic structure of the interface layer deviates from the bulk by measuring high-resolution photoelectron emission spectra of the Mn valence band close to an interface [1]. We use a compact pulsed laser deposition chamber attached to a photoelectron spectrometer at BL2C of the Photon Factory to grow a thick  $\text{La}_{1-x}\text{Sr}_x\text{MnO}_3$  (LSMO) film, covered by a thin layer of  $\text{La}_{1-x}\text{Sr}_x\text{FeO}_3$  (LSFO). The cover layer thickness is usually 1 to 3 unit cells. The probing depth of the photoelectron emission measurement is less than 10 unit cells. The contributions to the valence band spectrum by the bulk LSMO film and the thin LSFO cover layer can be separated by using a resonant emission technique, as shown in Fig. 1.

The intensity of the photoemission peak at 1 eV below the Fermi level is a direct measure of Mn 3d electron density

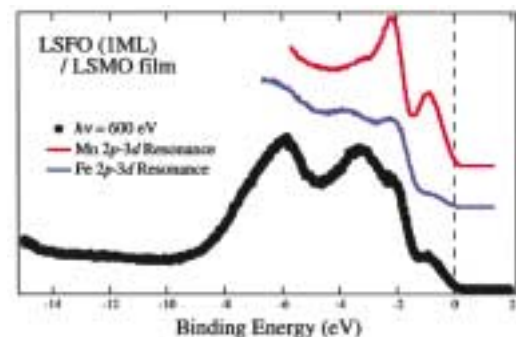


Fig. 1. Photoemission spectrum of a single unit cell film of  $\text{La}_{0.6}\text{Sr}_{0.4}\text{FeO}_3$  on a  $\text{La}_{0.6}\text{Sr}_{0.4}\text{MnO}_3$  surface. Resonant emission spectra of the valence band show the contribution of the Fe oxide layer and the top part of the bulk Mn oxide to the total emission intensity.

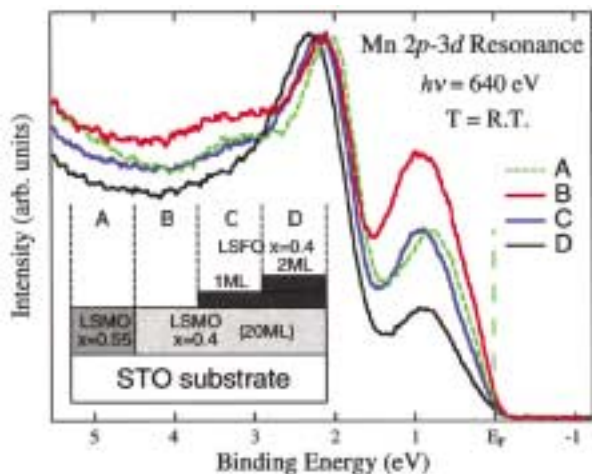


Fig. 2. Resonant Mn photoemission spectra of thick (A)  $\text{La}_{0.45}\text{Sr}_{0.55}\text{MnO}_3$  and (B)  $\text{La}_{0.6}\text{Sr}_{0.4}\text{MnO}_3$  films. A drop in the  $e_g$  state population in the topmost layer of the  $\text{La}_{0.6}\text{Sr}_{0.4}\text{MnO}_3$  film as a result of charge transfer to  $\text{La}_{0.6}\text{Sr}_{0.4}\text{FeO}_3$  can be seen in (C) and (D). The  $\text{La}_{0.6}\text{Sr}_{0.4}\text{FeO}_3$  cover layer thickness was 1 unit cell in (C) and 2 unit cells in (D).

in the  $e_g$  levels. For calibration purposes we have measured the intensity of this peak for a series of thin film samples with a different hole concentration  $x$ . A systematic drop in electron density is observed as the hole concentration  $x$  is increased, as shown by spectra (A) and (B) in Fig. 2.

A part of the LSMO ( $x=0.4$ ) film was covered with one or two monolayers of LSFO ( $x=0.4$ ) for charge transfer measurements at the LSMO/LSFO interface. A sketch of the sample geometry is shown in the inset in Fig. 2. As shown by spectrum (C) in Fig. 2, the presence of a single monolayer of LSFO on top of LSMO ( $x=0.4$ ), reduces the electron density to a level which corresponds to a bulk LSMO ( $x=0.55$ ) film. An even greater drop is observed when the thickness of the LSFO layer is doubled. This is a clear indication that there is indeed a large transfer of electrons from the Mn ions to Fe. The change in the effective carrier concentration is very large and can easily transform the topmost few unit cells of the LSMO film into an insulating or an antiferromagnetic phase.

#### Reference

[1] H. Kumigashira, K. Horiba, H. Ohguchi, K. Ono, M. Oshima, N. Nakagawa, M. Lippmaa, M. Kawasaki, H. Koinuma, *Appl. Phys. Lett.*, **82**, 3430 (2003).

#### Authors

H. Kumigashira<sup>a</sup>, K. Horiba<sup>a</sup>, M. Lippmaa, T. Ohnishi  
<sup>a</sup>Department of Applied Chemistry, University of Tokyo.

## Resonant Inverse Photoemission Study of Ni (110)

Y. Tezuka and S. Shin

Resonant inverse photoemission spectra (RIPES) of single crystal Ni was observed near Ni  $3p$  absorption edge. Ni is typical itinerant ferromagnet and it has nominal  $3d^9$  electronic structure. That is, the Ni has only one  $3d$  hole in conduction band. When it is magnetized, majority spin band is filled with electron, while minority spin band has one  $3d$  hole.

Inverse photoemission spectroscopy (IPES) observes the total density of state (DOS) of unoccupied state. Soft X-ray (SX) IPES have never been observed until recently, since its

intensity is extremely weak. On the other hand, Bremsstrahlung Isochromat Spectroscopy (BIS) in VUV and X-ray region is rather easy to observe, thus these spectra have been observed for many substances including single crystal Ni.

Figure 1 shows energy diagram of IPES. In normal process of IPES, incident electron undergoes transition to conduction band with emitting X-ray.

$$|d^n\rangle + e^- \rightarrow |d^{n+1}\rangle + h\nu \quad (1)$$

When the excitation energy is lower than absorption edge of core electron, only the normal process takes place. On the other hand, core electron is excited to conduction band or continuous energy level, when the energy of excitation electron is higher than absorption edge. In case that the excited electron is ejected to continuous level, higher-level electron (e.g. valence band) undergoes transition to core hole with emitting X-ray fluorescence. The fluorescence has typical energy for the substrate and does not vary with excitation energy. In other case that typically the excitation energy is the same as core absorption energy, intermediate excitation state  $|\underline{c}d^{n+2}\rangle$  is created without radiation. Then, the state decays with emitting X-ray.

$$|d^n\rangle + e^- \rightarrow |\underline{c}d^{n+2}\rangle \rightarrow |d^{n+1}\rangle + h\nu, \quad (2)$$

where  $\underline{c}$  denotes a core hole. Since the process (1) and (2) have same initial and final state, these two processes resonate with each other. In the case of Ni, however, nominal  $3d^9$  state cannot have  $3d^{n+2}$  state. Thus, the  $3d^9$  state would not be enhanced in the resonance. It is suggested from many experiments that Ni has other state;  $3d^{10}$  and  $3d^8$  [1, 2]. The  $3d^8$  state would be enhanced in the resonance.

We observed the Resonant IPES of single crystal Ni in SX region for the first time. Clean surface of Ni (110) was obtained by Ar-ion bombardment and annealing at temperature of about 700°C. Cleanness of the sample was checked by Auger spectra and LEED measurement.

Figure 2 shows resonant IPES spectra of Ni (110). On (66.0 eV) and off (71.9 eV) resonant spectra are shown. Ni  $3d^9$  fluorescence peak that have energy of about 65.5 eV is observed in both spectra. The main peak just above  $E_F$  is Ni  $3d$  structure, while Ni  $4sp$  is observed at 10~15 eV. Though the  $3d$  and  $4sp$  band show band dispersion, it cannot be discussed here, because the excitation electron is not normal incidence and the wave vector of electron is larger than zone boundary. The  $3d$  band structure becomes weak in the resonant spectra. This fact means the  $3d$  structure originated from  $3d^9$  components. Satellite structures are also observed

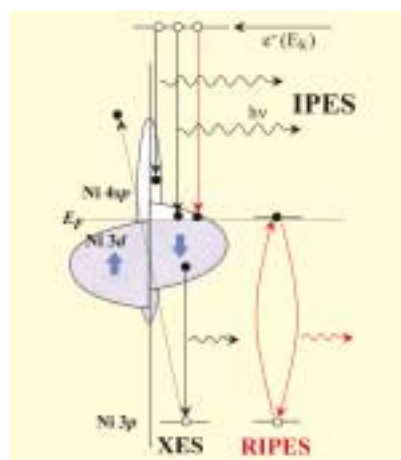


Fig. 1. Energy diagram of IPES. Core electron is excited to conduction band or continuous energy level, when the energy of excitation electron is higher than binding energy of core electron.

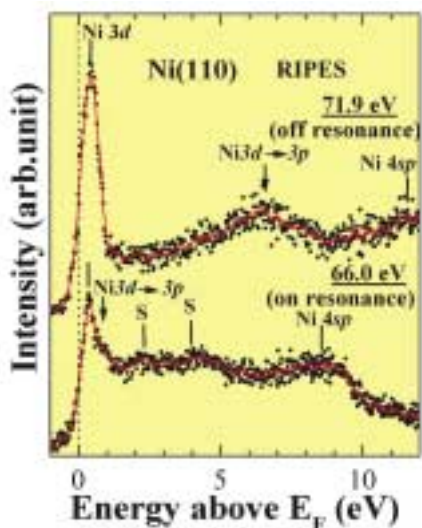


Fig. 2. RIPES spectra of Ni (110). On (66.0 eV) and off (71.9 eV) resonant spectra are shown. Dots are observed data and red lines are smoothed data. Ni 3d3p fluorescence peak is observed in both spectra. Main peak just above EF is Ni 3d band, while Ni 4sp band observed at 10–15 eV. Satellite structures are observed at about 2 and 4 eV in resonant spectra.

at about 2 and 4 eV in resonant spectra. We have observed the IPES of polycrystalline Ni that was prepared by evaporation method. In those spectra, Ni 3d band was observed rather wide and Ni 4sp band could not be observed.

Tanaka and Jo calculated RIPES spectra of Ni on the basis of the Anderson impurity model. In their calculation, Ni has 10–20 %  $3d^8$  ground state. They suggested that two satellite structures should be observed at about 2 and 4 eV and these are enhanced at the Ni 3p core threshold [3]. In our spectra, satellite structures are observed at about 2 and 4 eV, though the intensities are very weak. We think these satellite structures originate from the  $3d^8$  component. The RIPES spectra in this study give us a direct evidence of  $3d^8$  component in Ni metal.

#### References

- [1] T. Jo and G. A. Sawatzky, Phys. Rev. B **43**, 8771 (1991).
- [2] G. van der Laan and B. T. Thole, J. Phys. Condens. Matter **4**, 4181 (1992).
- [3] J. Phys. Soc. Jpn, **66**, 1591 (1997).

#### Authors

Y. Tezuka<sup>a</sup>, D. Nakajima<sup>a</sup>, Y. Miyazaki<sup>a</sup>, K. Kanai<sup>b</sup>, H. Ishii<sup>c</sup>, S. Nozawa<sup>d</sup>, R. Eguchi, S. Shin  
<sup>a</sup>Department of Science and Technology, Hirosaki University  
<sup>b</sup>Department of Science, Nagoya University  
<sup>c</sup>Taiwan APCSCT  
<sup>d</sup>Photon Factory, KEK

## Ultrahigh-Resolution Photoemission Spectroscopy of The Binary $Cd_{5.7}Yb$ and Its Crystalline Approximant $Cd_6Yb$

R. Tamura and S. Shin

The recently discovered stable binary  $Cd_{5.7}Yb$  quasicrystal (i-phase) [1] is of particular interest from the view of PE spectroscopy: First, there exists a cubic crystalline approximant ( $1/1-Cd_6Yb$ ) in the vicinity of the i-phase composition, thus enabling us to investigate the influence of quasiperiodicity on the electronic structure. Second, since it contains a rare-earth element whose  $4f$  states lie close to  $E_F$  [2] and such well localized  $4f$  states are likely to produce sharp

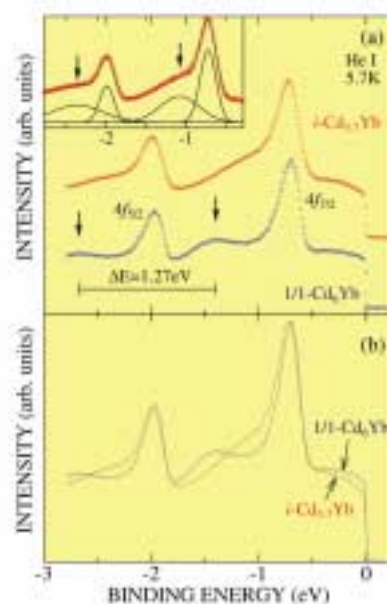


Fig. 1. (a) Low-temperature He-I PE spectra of  $i-Cd_{5.7}Yb$  and  $1/1-Cd_6Yb$  with an energy resolution of 20 meV. The inset shows deconvolution of the  $i-Cd_{5.7}Yb$  spectrum. (b) The same spectra superimposed on one another for a better comparison.

final-state multiplet structures in the PE spectrum, we expect that surface sensitive PE technique allows us to investigate changes of the electronic structure in the surface region of the solid with high resolution [3].

Figure 1 (a) presents low-temperature PE spectra for  $i-Cd_{5.7}Yb$  and  $1/1-Cd_6Yb$  measured at 5.7 K and in Fig.1(b) are shown the same spectra superimposed on one another in order to clarify the difference between the two compounds. First of all, a common feature is observed in both spectra of  $i-Cd_{5.7}Yb$  and  $1/1-Cd_6Yb$ : Two distinct peaks appear around  $BE = -0.7$  and  $-2.0$  eV. Comparing with the theoretical DOS of  $1/1-Cd_6Yb$  [2], the observed peaks can be readily assigned to the Yb  $4f$  states. This is further confirmed by the fact that the estimated energy separation of 1.27 eV between the peaks corresponds exactly to the atomic spin-orbit energy 1.27 eV and hence we conclude that the peaks are due to the  $4f_{7/2}$  and  $4f_{5/2}$ -derived states as appropriate. In Fig.1(b), we notice that the peak positions of the Yb  $4f$  doublet are deeper for the i-phase than for the approximant, by about  $25 \pm 5$  meV. This implies that the electronic system around Yb atoms is more stable in the i-phase than in the approximant.

A striking feature in Fig.1 is the existence of two humps at higher binding energies side of the corresponding  $4f$  peaks, as clearly seen at around  $BE = -1.4$  eV and  $-2.7$  eV for the approximant while they are mixed with the doublet of the  $4f$  states for the quasicrystal. The locations of the humps were determined to be  $-1.40 \pm 0.01$  and  $-2.68 \pm 0.01$  eV for  $1/1-Cd_6Yb$  and  $-1.08 \pm 0.05$  and  $-2.37 \pm 0.05$  eV for  $i-Cd_{5.7}Yb$ . In rare-earth-metal compounds, such extra humps in the vicinity of well localized states such as the  $4f$  states are well known for the surface core-level shifts (SCS), which reflect changes of the electronic structure in the surface region. The energy separation of the humps is about 1.3 eV for both compounds and agrees well with the  $4f$  splitting energy of the bulk states, confirming that they are due to the  $4f$ -derived states. The lowering of the binding energy at the surface indicates that the binding energies of surface atoms

are higher than those of bulk atoms. The surface components are shifted to higher binding energies by  $0.68 \pm 0.01$  eV for  $1/1$ - $\text{Cd}_6\text{Yb}$  and by  $0.36 \pm 0.05$  eV for  $i$ - $\text{Cd}_{5.7}\text{Yb}$ . The existence of the SCS themselves unambiguously verifies that the electronic structure at the surface is different from that in the bulk in the case of the quasicrystal and the approximant. The present experiment is the first direct observation of the surface states in the quasicrystalline materials.

Next we focus on the structure in the vicinity of  $E_F$  in the PE spectra. As seen from Fig.1(a), a decrease of the spectral intensity towards  $E_F$  which is well distinguished from the Fermi cut-off is observed for both phases and this trend becomes enhanced near  $E_F$ . Moreover, the intensity depression at  $E_F$  is found to be considerably stronger for the  $i$ -phase than for the approximant (Fig.1(b)), which clearly shows that the dip at  $E_F$  is deeper in the quasicrystal than in the cubic approximant. The stronger intensity decrease near  $E_F$ , i.e. less occupied states in the vicinity of  $E_F$ , in  $i$ - $\text{Cd}_{5.7}\text{Yb}$  directly indicates a larger energy gain due to the dip formation in the  $i$ -phase than in the approximant.

#### References

- [1] A.P. Tsai *et al.*, Nature **408**, 537 (2000).
- [2] Y. Ishii *et al.*, Phys. Rev. Lett. **87**, 206408 (2001).
- [3] R.Tamura *et al.*, Phys. Rev. B **65**, 224207 (2002).

#### Authors

R. Tamura<sup>a</sup>, Y. Murao<sup>a</sup>, S. Takeuchi<sup>a</sup>, T. Kiss, T. Yokoya, and S. Shin  
<sup>a</sup>Department of Materials Science and Technology, Tokyo University of Science

## Discovery of Missing Link: IV. Spin-1/2 Spinel Oxide $\text{MgTi}_2\text{O}_4$

N. Nakayama and Y. Ueda

The spinel oxides  $\text{AB}_2\text{O}_4$  have displayed a variety of electromagnetic properties such as superconductivity, heavy fermion behavior, charge order, and unusual magnetic properties. One important structural property of the cubic spinel structure is a three-dimensional (3D) network of corner-sharing tetrahedra formed by B-cations (pyrochlore lattice). This structural feature has drawn much attention as a geometrically frustrated 3D lattice. An antiferromagnetic

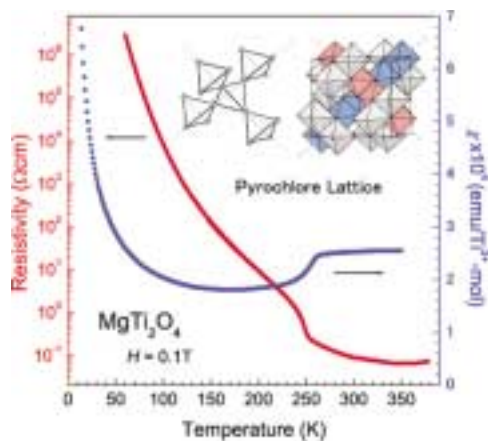


Fig.1. Temperature dependence of magnetic susceptibility and resistivity for  $\text{MgTi}_2\text{O}_4$ .  $\text{MgTi}_2\text{O}_4$  shows a transition from metal to spin-singlet insulator at 260 K. This transition is accompanied by a structural change from cubic to tetragonal. The inset is a schematic illustration of the spinel structure composed of  $\text{BO}_6$  octahedra in  $\text{AB}_2\text{O}_4$  and a three-dimensional network of corner-sharing tetrahedra formed by B-cations (pyrochlore lattice). The dotted line indicates a certain chain of edge-sharing  $\text{BO}_6$  octahedra.

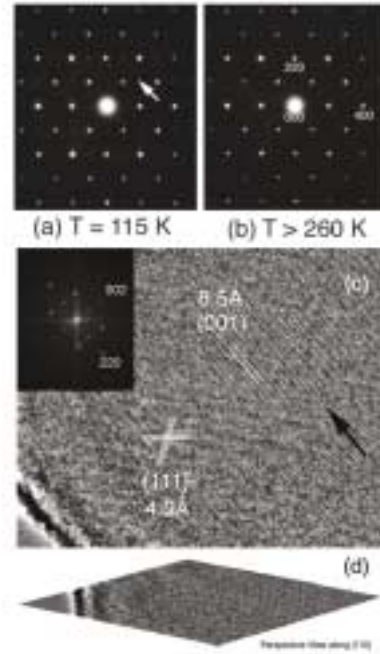


Fig. 2. [110]-zone electron diffraction patterns below (a) and above (b) the transition temperature (260 K) in  $\text{MgTi}_2\text{O}_4$ . The lattice image (c) of the low temperature phase shows clear lattice fringes of the fundamental spinel lattice. It also shows (001) lattice fringes as marked by an arrow. The perspective view (d) of the image (c) along the  $[1-10]$  direction reveals that the (001) lattice fringes appear almost whole the observed region but with several defects.

exchange interaction among Heisenberg spins on the neighboring B-cations maximizes frustration in the magnetic order. Such geometry of the crystal structure also produces strong frustration in charge ordering.

It is well known that quantum effects on spin fluctuations are markedly enhanced in the  $S=1/2$  ( $d^1$ ) system. Very recently, the exotic quantum ground state was theoretically predicted on the pyrochlore lattice with  $S=1/2$ . Although the search for a spin-1/2 compound has been motivated by its intriguing quantum phenomena, it has been missing in the spinel family.

We have succeeded in synthesizing  $\text{MgTi}_2\text{O}_4$  that have been expected to realize the pyrochlore lattice with  $S=1/2$ , and investigated the structural and electromagnetic properties. We found a metal-insulator transition at 260 K (Fig. 1) [1]. The ground state could be spin singlet, because the magnetic susceptibility obtained by subtracting the Curie tail at low temperature is comparable to that for other spin-gap systems and there is no evidence for magnetic order in  $\mu\text{SR}$  experiments. The transition is accompanied by a structural transition from cubic to tetragonal. Shown in Fig. 2 are the change of the electron diffraction pattern below and above 260 K and the high-resolution TEM lattice image of the low temperature phase. The electron diffraction pattern at 115 K shows very weak superlattice spots in addition to the fundamental spots (Fig. 2(b)) of spinel lattice, indicating the symmetry breaking. They appear only at the forbidden reciprocal lattice points of the cubic spinel and no spot indicating the multiplicity of the supercell was observed.

These results indicate a Peierls-like transition in  $\text{MgTi}_2\text{O}_4$ . Why does the Peierls-like transition inherent in 1D system occur in the 3D spinel system? As a possible scenario, an orbital ordering might play an important role in the Peierls-like transition of  $\text{MgTi}_2\text{O}_4$ . In the cubic spinel structure, the  $\text{TiO}_6$  octahedra are arranged in chains through edge sharing, as shown in the inset of Fig. 1. If there exists orbital

ordering along each chain direction, the dimensionality is lowered from 3D to 1D, which is responsible for the Peierls transition.

#### Reference

[1] M. Isobe and Y. Ueda, *J. Phys. Soc. Jpn.* **71**, 1848 (2002).

#### Authors

N. Nakayama<sup>a</sup>, M. Isobe, M. Ichihara, and Y. Ueda

<sup>a</sup>Faculty of Engineering, Yamaguchi University

## Room Temperature Synthesis of Carbon Nanotubes by Electrochemical Deposition using Organic Solution

H. Yokomichi, M. Ichihara and F. Sakai

Carbon nanotubes have been commonly synthesized using a wide variety of chemical vapor deposition (CVD) methods [1,2]. As the vapor phase synthesis, arc discharge and laser ablation techniques have also been used for nanotube synthesis. In addition, an arc discharge [3] and thermal CVD [4] under high magnetic field of 10 T have been employed for nanotube synthesis. However, synthesis temperature of nanotubes by the methods, at least 550 °C, is higher than that of graphite-like carbon films. In the present study, we show room temperature synthesis of carbon nanotubes and carbon nanowires, for the first time, by an electrochemical deposition technique under a liquid phase of organic solution using a metal catalyst. Nanocarbons with sea urchin-like and onion-like structures have also been successfully synthesized using the electrochemical technique.

Electrochemical deposition has been carried out by applying a DC voltage in organic solutions such as CH<sub>3</sub>OH and C<sub>2</sub>H<sub>5</sub>OH. The p-type crystalline silicon (c-Si) was used for the substrate. A graphite rod and the c-Si substrate were used for a cathode and an anode, respectively. The metal catalyst was dissolved into the solution.

The c-Si substrates colored dark black after the electrochemical deposition with and without the metal catalyst. SEM images of the deposits without Ni catalyst indicate that amorphous carbon films with a roughened surface and

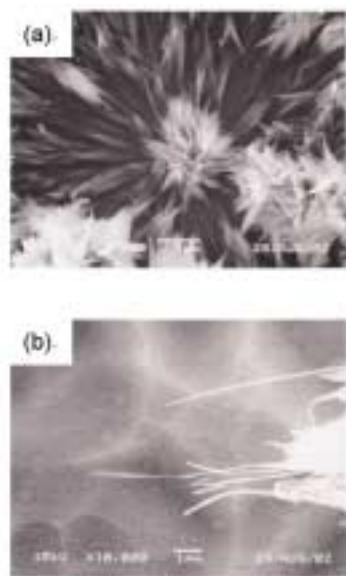


Fig. 1. SEM images of various nanocarbons: sea urchin-like structures (a) and nanowires (b) synthesized using C<sub>2</sub>H<sub>5</sub>OH with a Ni catalyst. The metal catalyst was dissolved into the solution.

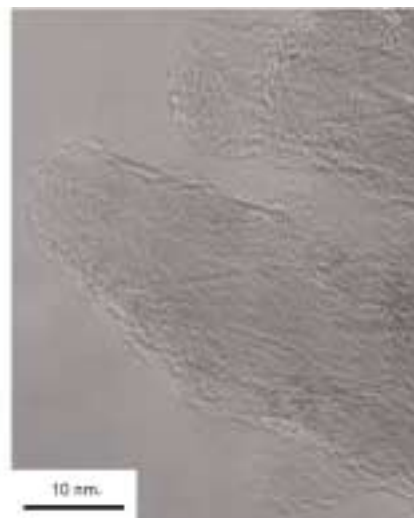


Fig. 2. TEM image of the deposits synthesized using C<sub>2</sub>H<sub>5</sub>OH with a Ni catalyst. The metal catalyst was dissolved into the solution.

graphite grains of a few micron sizes were deposited on the substrate. The carbon nanotubes and nanowires were not discernable for all the case. On the contrary, nanocarbons with various structures, e.g., sea urchin-like structures (a) and nanowires (b), were observed for the deposits using C<sub>2</sub>H<sub>5</sub>OH with Ni(NO<sub>3</sub>)<sub>n</sub>·mH<sub>2</sub>O as shown in Figs. 1 (a) and (b), depending areas of the samples. The existence of carbon nanotubes is shown by the TEM image in Fig. 2 for the deposits using C<sub>2</sub>H<sub>5</sub>OH with the metal catalyst, although carbon nanotubes were not discernable for the deposits without the catalyst.

Although the growth mechanism is not clear, we speculate that the metal anions are attached on the c-Si substrate at an initial stage and then the metal grains act as a nucleation and growth centers of nanocarbons. In fact, the metal films were grown for a shorter time, when the solution with much more metal anions was used. Therefore, nanocarbons are grown from carbon anions generated by the applied high electric field by the aid of metal grains created in the initial stage. The Ni metals were detected by EDS measurements for the regions corresponding to the SEM images shown in Figs. 1 (a) and (b). However, the Ni grains were not explicitly discernable by electron reflection images for the regions corresponding to the SEM images. These results suggest that the metal grain sizes are small, e.g., below a few tens of nm. The growth for various types of nanocarbons may be attributed to shapes of the metal grains determined by the strength of applied electric fields and the surface morphology of the substrate, because the types of nanocarbons have been reported to depend on the size of metal grains in the case of thermal CVD [5].

We would like to thank Dr. N. Kishimoto of National Institute for Materials Science for useful suggestions.

#### References

- [1] W. Li et al., *Science* **274**, 1701 (1996).
- [2] M. Terrones et al., *Nature* **388**, 52 (1997).
- [3] H. Yokomichi, H. Sakima, M. Ichihara, F. Sakai, K. Itoh and N. Kishimoto, *Appl. Phys. Lett.* **74**, 1827 (1999).
- [4] H. Yokomichi, F. Sakai, M. Ichihara and N. Kishimoto, *Transactions of the Materials Research Society of Japan*, in press.
- [5] H. Yokomichi, F. Sakai, M. Ichihara and N. Kishimoto, *J. Non-Cryst. Solids* **299-302**, 868 (2002).

#### Authors

H. Yokomichi<sup>a</sup>, M. Ichihara and F. Sakai

<sup>a</sup>Department of Electronics and Informatics, Toyama Prefectural University.

# X-ray and Optical Studies on One-Dimensional Organic Conductors

T. Kawamoto, T. Mori, J. Yamaura, and H. Tajima

Several TTP series donors [tetrathiapentalene (TTP) series donors] with methylthio groups realize one-dimensional electronic states owing to the side-by-side steric hindrance of the methylthio groups [1]. (ChTM-TTP)<sub>2</sub>X (X=GaCl<sub>4</sub>, AuBr<sub>2</sub>, and Au(CN)<sub>2</sub>) are quasi-one-dimensional organic conductors with dimerized donor stacking structures [2,3]. The crossover from a metal to a charge localized state takes place around 150 K (for the GaCl<sub>4</sub> salt), followed by an antiferromagnetic transition at 32 K [3]. (ChTM-TTP)<sub>2</sub>X is the first TTP conductor whose ground state is an antiferromagnetic insulator. Although these physical properties resemble (TMTTF)<sub>2</sub>Br, the charge localization temperature and the Néel temperature are much higher than those of the TMTCF salts.

Low-temperature crystal structure and optical properties of the quasi-one-dimensional organic conductor (ChTM-TTP)<sub>2</sub>GaCl<sub>4</sub> have been investigated at the X-ray laboratory and the Spectroscopy laboratory in the Materials Design and Characterization Laboratory. As the temperature lowers, the disordered anion structure transforms to an ordered state with a superstructure wave vector of  $q=(1/2, 0, 1/2)$  (Fig.1). The peak intensities of the superlattice gradually increase in the metallic region, and are saturated below 150 K; this indicates that the charge localization below 150 K is independent of the superlattice. The reflectance spectra of (ChTM-TTP)<sub>2</sub>X suggest the existence of moderate interchain interactions (Fig.2). The transverse interactions are more pronounced in the GaCl<sub>4</sub> salt ( $t_{\perp}/t_{\parallel} \approx 1/7$ ) than the AuBr<sub>2</sub> and Au(CN)<sub>2</sub> salts. The low-temperature optical reflectance of the GaCl<sub>4</sub> salt shows no significant change, indicating that (ChTM-TTP)<sub>2</sub>GaCl<sub>4</sub> goes to an insulating state with a small energy gap, in consistent with the transport property. The low-frequency peak in the chain-axis optical conductivity is attributed to electron correlation,

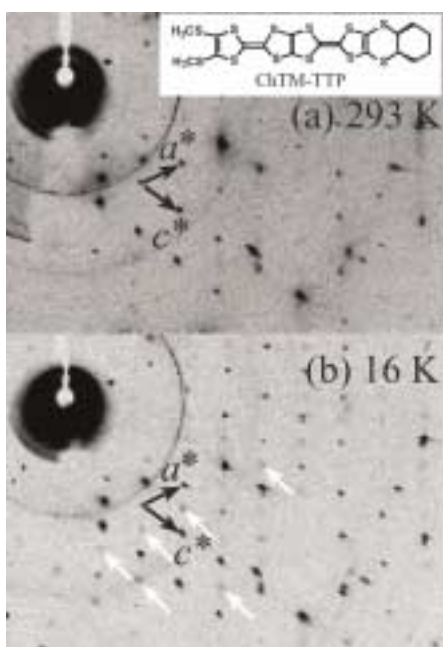


Fig. 1. X-ray oscillation photograph of (ChTM-TTP)<sub>2</sub>GaCl<sub>4</sub> at room temperature (a) and 16 K (b) showing the  $q=(1/2, 0, 1/2)$  scattering (white arrows). The original axes are shown by black arrows.

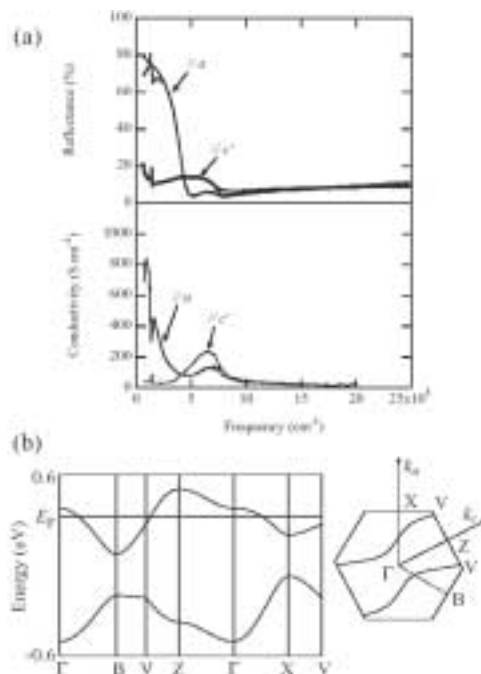


Fig. 2. (a) Reflectance spectra and optical conductivities of (ChTM-TTP)<sub>2</sub>GaCl<sub>4</sub> at room temperature. The solid lines in upper figure are the Drude-Lorentz fits. (b) Energy band structure and the Fermi surface of (ChTM-TTP)<sub>2</sub>GaCl<sub>4</sub> calculated from the transfer integrals obtained through the optical experiment at room temperature.

though the expected on-site Coulomb repulsion  $U$  is relatively small. This scenario is consistent with the antiferromagnetic ground state of (ChTM-TTP)<sub>2</sub>X.

## References

- [1] T. Mori et al., Mol. Cryst. Liq. Cryst. **284**, 271 (1996).
- [2] M. Ashizawa et al., Chem. Lett. 649 (1997).
- [3] T. Kawamoto et al., Bull. Chem. Soc. Jpn. **75**, 435 (2002).

## Authors

T. Kawamoto<sup>a</sup>, M. Ashizawa<sup>a</sup>, T. Mori<sup>a</sup>, T. Yamamoto, J. Yamaura, and H. Tajima  
<sup>a</sup>Department of Organic and Polymeric Materials, Tokyo Institute of Technology

## The Magnetization Plateau and Commensurate - Incommensurate Transition in the 2D Triangular Antiferromagnet Cs<sub>2</sub>CuBr<sub>4</sub>

Y. Fujii and M. Takigawa

The quasi-two dimensional antiferromagnet Cs<sub>2</sub>CuBr<sub>4</sub>, where the magnetic Cu<sup>2+</sup> ions with  $S=1/2$  form a distorted triangular lattice in the  $bc$ -plane, has attracted keen attention, since a plateau was observed in the magnetization curve at one-third of the saturation magnetization when the magnetic field was applied along the  $b$ - or  $c$ -axes [1]. Recent neutron diffraction experiments suggested a cycloidal incommensurate spin ordering propagating along the  $b$ -axis with  $T_N=1.4$  K at zero field. In order to obtain microscopic insight into the spin structure and the spin dynamics in Cs<sub>2</sub>CuBr<sub>4</sub>, we have performed <sup>133</sup>Cs NMR experiments in the temperature range down to 0.4 K under the magnetic field up to 15.9 T. A single crystal of Cs<sub>2</sub>CuBr<sub>4</sub> (2 mm×3 mm×4 mm) was used.

Figures 1 [A] and [B] show the NMR spectra obtained for the magnetic fields applied along the  $b$ - and  $a$ -axis,

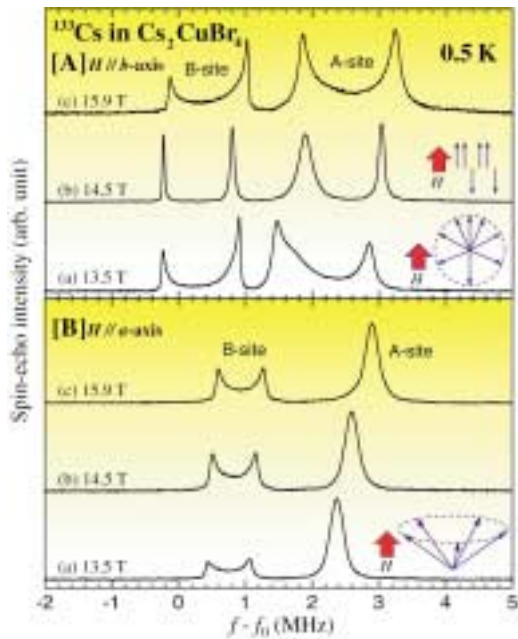


Fig. 1. The NMR spectra of  $^{133}\text{Cs}$  nuclei in  $\text{Cs}_2\text{CuBr}_4$  for the magnetic field along the [A]  $b$ - and [B]  $a$ -axis. Only the spectrum [A](b) obtained in the plateau phase shows discrete resonance lines, while others exhibit continuous spectra. The proposed spin structure is shown for each spectrum.

respectively. Note that the spectrum [A]-(b) was measured in the  $1/3$ -plateau phase, which occurs for the field range 14.0-15.5 T for  $H//b$  [1], while the others were obtained outside the plateau. In all cases, we observed two distinct  $^{133}\text{Cs}$  resonance lines, which correspond to two inequivalent sites, A and B, in the unit cell, although we have been yet unable to assign each line to a specific cesium site.

The spectra in Fig. 1A(a) and A(c) for  $H//b$  outside the plateau show a characteristic double-horn type line shape with a continuum of finite intensity between two peaks. Generally, such line shape is a signature of an incommensurate structure, in which the magnetic hyperfine fields at nuclei have a sinusoidal modulation yielding a continuum. The peaks of the spectra correspond to the extrema of the modulation. The fact that the spectra are asymmetric is explained if the field is in the cycloidal spin plane. Since the spins should be more densely populated along the field direction (Fig. 1[A](a)), we expect a distortion from purely sinusoidal hyperfine field modulation, resulting in an

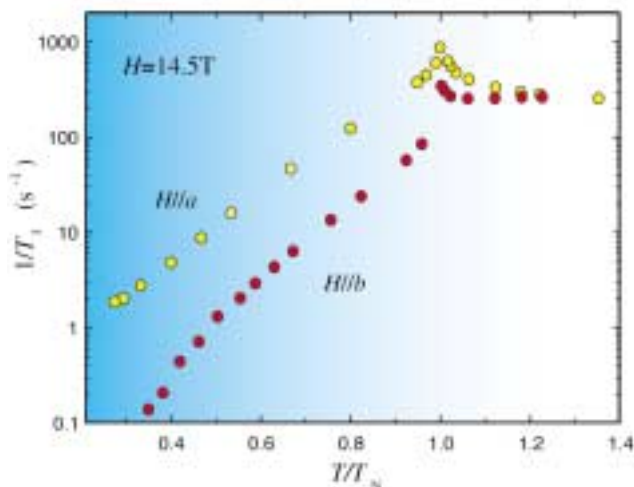


Fig. 2. Temperature dependence of the spin-lattice relaxation rate at 14.5 T inside ( $H//b$ ) and outside ( $H//a$ ) the plateau phase.

asymmetric line shape.

Such a continuum is absent for the spectrum in the plateau region shown in Fig. 1[A](b). The spectrum consists only of two nearly symmetric discrete peaks with the intensity ratio approximately 1:2 for both A and B-sites. This result provides strong evidence that collinear up-up-down commensurate spin structure is realized in the  $1/3$ -plateau phase.

In contrast, the spectra for the B-sites obtained for  $H//a$  (Fig. 1[B]), where the magnetization plateau was not observed, show symmetric double-horn type structure for all fields, indicating persistence of the incommensurate structure for the entire field range. The symmetric line shape suggests cone-type spin structure shown in Fig. 1[B], where the modulation of the hyperfine field is purely sinusoidal. It should be noted that, even though the cycloidal spin component is perpendicular to the field, anisotropic hyperfine interaction generally produces parallel component of the hyperfine field. The A-sites, on the other hand, show a sharp single peak, presumably because the anisotropy of the hyperfine interaction is not large enough.

The spin-lattice relaxation rates ( $1/T_1$ ) measured at 14.5 T inside ( $H//b$ ) and outside ( $H//a$ ) the plateau phase are plotted against  $T/T_N$  ( $T_N$ : the Neel temperature) in Fig. 2. The relaxation rates decrease much more steeply for  $H//b$  than for  $H//a$ , indicating different low lying excitation spectra for commensurate and incommensurate phases. In particular, the slow decrease for  $H//a$  at low temperatures is presumably due to gapless phase fluctuations in the incommensurate structure.

#### Reference

[1] H. Tanaka *et al.*: Phys. Rev. B **67**, 104431 (2003).

#### Authors

Y. Fujii<sup>a</sup>, T. Nakamura<sup>a</sup>, M. Chiba<sup>a</sup>, H. Kikuchi<sup>a</sup>, T. Goto<sup>b</sup>, K. Kodama, S. Matsubara, and M. Takigawa  
<sup>a</sup>Department of Applied Physics, Fukui University  
<sup>b</sup>Graduate School of Human and Environmental Studies, Kyoto University

## Accurate Dynamic Structure Factor of the Homogeneous Electron Liquid

H. Yasuhara and Y. Takada

The electron liquid, an assembly of  $N$  electrons embedded in a uniform positive background, has been studied to clarify the nature of electron correlation in metals, putting aside the influence of the periodic ion potential. This simplified model poses us a tough problem, but after the struggles lasting longer than half a century, accurate knowledge of its almost all static properties is now acquired by a number of sophisticated methods including quantum Monte Carlo simulations over the entire region of metallic densities  $1.88 < r_s < 5.6$  where  $r_s$  is the conventional density parameter.

As for dynamical properties, on the other hand, our knowledge is still not enough in spite of all previous efforts to go beyond the random-phase approximation (RPA) in an attempt to explain the double-peak structure in the dynamical structure factor  $S(\mathbf{q}, \omega)$  observed in light metals like Al. Among approximation schemes, the Baym-Kadanoff (BK) conserving one formulated in terms of the full Green's function  $G$  is most suitable for the evaluation of  $S(\mathbf{q}, \omega)$ . Accuracy of the result depends critically on the choice of the

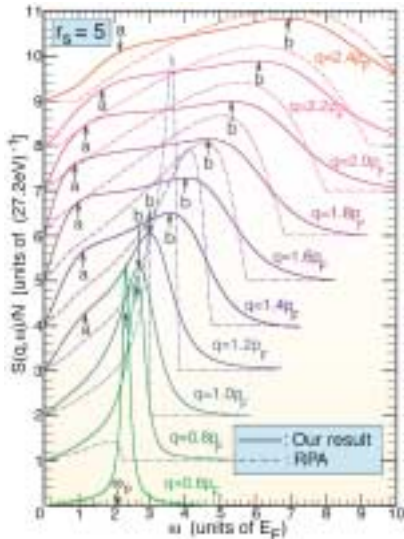


Fig. 1. Dynamical structure factor of the electron liquid at  $r_s=5$ . The value indicated by  $\omega_p$  is the plasmon energy at  $q=0$ . The excitonic effect manifests itself in the structure indicated by  $a$ .

energy functional  $\Phi[G]$ , but the result will never become exact, since no algorithm is known to give the exact  $\Phi[G]$ .

A conceptually different scheme is developed to obtain the exact  $S(q, \omega)$  [1]; instead of pursuing  $\Phi[G]$ , we pay attention to the exact functional relations between the self-energy  $\Sigma$  and the vertex function  $\Gamma$ , obeying the microscopic conservation law. In particular,  $\Gamma$  is determined by the Bethe-Salpeter equation with an irreducible electron-hole interaction given by the functional derivative,  $\delta\Sigma/\delta G$ . Starting from an arbitrary input, we iteratively revise both  $\Sigma$  and  $\Gamma$  simultaneously towards self-consistency through the relations, whereby the number of terms representing  $\Sigma$  generated in this iterative process rapidly increases, eventually covering all terms derivable from the exact  $\Phi[G]$  when the self-consistency is achieved.

In a numerical algorithm, however, the functional differentiation  $\delta\Sigma/\delta G$  is not feasible. Thus we need to invent an alternative scheme to revise  $\Gamma$  on a computer accurately and efficiently. Recently a physically motivated and accurate enough prescription is given for  $\Gamma$  [2], enabling us to obtain the result of  $S(q, \omega)$  [3] that is most accurate among all existing ones.

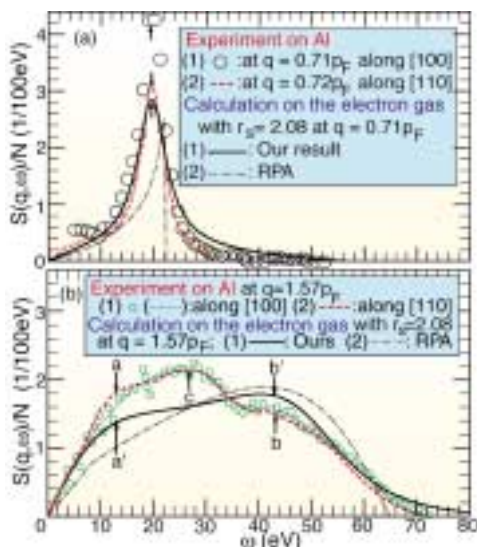


Fig. 2. Comparison between  $S(q, \omega)$  of the electron liquid at  $r_s=2.08$  and the experimental one for Al metal.

Throughout the metallic-density region, qualitative features of  $S(q, \omega)$  remain the same; a typical example at  $r_s=5$  is given in Fig. 1. Besides a broad peak  $b$  located at almost the same position in the RPA, there appears a clear shoulder  $a$  accompanied by a steepened slope of the linear term in  $S(q, \omega)$  for small  $\omega$ . The peak  $b$ , being identified as “the center of gravity” of one-pair excitations, is transformed continuously into the plasmon peak as  $|q|$  decreases. The shoulder  $a$  is well developed particularly for  $1.4 < |q|/p_F < 2$  and the slope is surprisingly enhanced over the RPA value accordingly. These features imply inseparable coupling between one- and multi-pair excitations in the one-pair excitation region, attractive electron-hole multiple scattering (excitonic effect) on the low- $\omega$  side of the one-pair region, and extra contributions from multi-pair excitations outside of it.

Since accurate knowledge of  $S(q, \omega)$  of the electron liquid is now available, we have compared it with the experimental one for Al, a metal regarded as most electron-liquid-like with  $r_s=2.08$ , in order to see how the band effects modifies the actual structure of  $S(q, \omega)$ . The result of comparison is shown in Fig. 2, which leads us to conclude that the electron-liquid model applies well to Al on the whole and especially so for  $\omega < E_F$  ( $\sim 11\text{eV}$ ). The discrepancy from the model at higher  $\omega$  is ascribed to the strong tight-binding nature of unoccupied  $3d$  and  $4f$  bands in Al, leading to the structure  $c$  in Fig. 2.

#### References

- [1] Y. Takada, Phys. Rev. B **52**, 12708 (1995).
- [2] Y. Takada, Phys. Rev. Lett. **87**, 226402 (2001).
- [3] Y. Takada and H. Yasuhara, Phys. Rev. Lett. **89**, 216402 (2002).

#### Authors

Y. Takada and H. Yasuhara<sup>a</sup>

<sup>a</sup>Institute for Materials Research, Tohoku University.

## Magnetic Field-Induced Transition from a Spin Jahn-Teller Antiferromagnet to a 3-1 Spin Ordered State in Geometrically Frustrated Chromium Spinel

H. Ueda and T. Goto

It is well known that antiferromagnetism on the pyrochlore lattice is a subject of strong frustration, giving rise to highly degenerate magnetic ground states. To lift the gigantic degeneracy, the system often experiences a structural phase transition at low temperatures, which may be viewed as a spin Jahn-Teller effect. In the presence of magnetic field, however, the situation should be altered substantially. We might expect the formation of completely different spin ordering pattern produced by the interplay between the frustration and the field induced spin alignment. This spin state transition is likely accompanied with the structural phase transition.

The  $\text{CdCr}_2\text{O}_4$  oxide with the normal spinel structure is one of the best defined spin Jahn-Teller systems together with  $\text{ZnCr}_2\text{O}_4$ . A magnetic ordering in  $\text{CdCr}_2\text{O}_4$  is marginally achieved by experiencing a structural transition from cubic to tetragonal at 7.8 K. From the high temperature susceptibility, the Weiss temperature  $\Theta$  is estimated to be  $-70$  K. For the chromium ion with  $S=3/2$ , a magnetic field of 1 T corresponds to a temperature of 2 K. This implies that the energy scale of magnetic interaction in  $\text{CdCr}_2\text{O}_4$  is com-

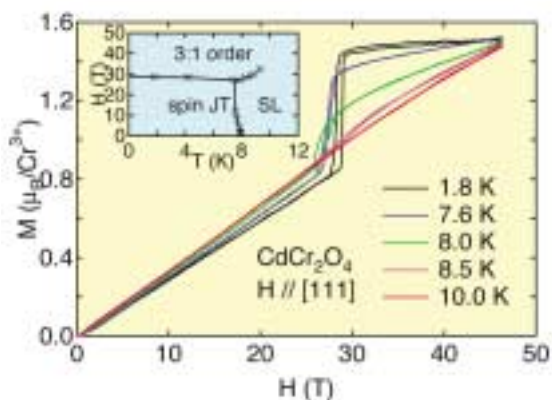


Fig. 1. Temperature dependence of the magnetization curve of  $\text{CdCr}_2\text{O}_4$  for the [111] direction. At low temperatures, a metamagnetic step at 28 T with a preceding plateau region is observed. A clear hysteresis behavior indicates first-order transition. Although the step feature becomes broad with increasing temperature, it should be noted that the transition takes place above  $T_N = 7.8$  K. The inset shows the  $H$ - $T$  phase diagram up to 46 T.

parable to that of an experimentally achievable magnetic field of several tens Tesla. Taking the advantage of relatively small magnetic interaction, we explored field-induced phase transitions using pulsed high magnetic fields at ISSP.

We found a novel metamagnetic transition in  $\text{CdCr}_2\text{O}_4$ . The magnetization curve for 1.8 K shows a discontinuous jump around 28 T, followed by a magnetization plateau as shown in Fig. 1. The magnetization jump shows a hysteresis, indicating that it represents a first-order transition. This transition is accompanied by a jump of the magnetostriction. Considering the absence of spin-orbit coupling, this relatively large magnetostriction is surprising. We believe that this implies a strong spin-lattice coupling enhanced by a frustration.

The magnetic moment at the plateau is  $1.5 \mu_B/\text{Cr}^{3+}$ , which is exactly one half of the full moment of  $\text{Cr}^{3+}$  ( $S = 3/2$ ). One half plateau can be naturally understood by considering three up and one down configuration of four spins on each tetrahedron, which may be considered as three dimensional analogue of the  $1/3$  magnetization plateau in triangular antiferromagnets. There are two possible spin structures. One has a rhombohedral symmetry ( $R3m$ ), in which ferromagnetic kagomé and triangular layers are antiferromagnetically stacked along the [111] direction, as shown in Fig. 2. The other has a cubic symmetry ( $P4332$  or  $P4132$ ) with down spins occupying the next nearest site.

The temperature dependence of the novel field-induced transition was measured. In low fields, a discontinuous change of the slope is clearly observed between 7 K and 8 K, which corresponds to the antiferromagnetic (spin Jahn-

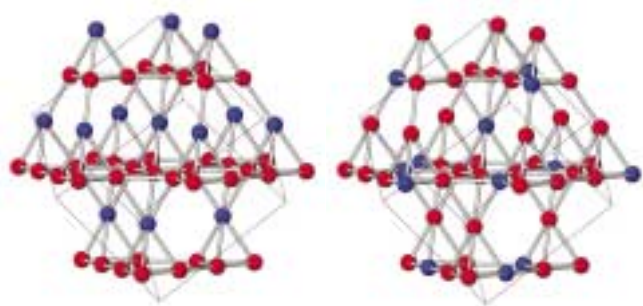


Fig. 2. Two possible configurations in the plateau phase. Red circles correspond to up-spins and blue circles to down-spins. The left structure is cubic ( $P4332$ ) and the right one is rhombohedral ( $R3m$ ).

Teller) transition. It should be emphasized that even above the antiferromagnetic transition temperature, the first-order transition to the 3-1 state can clearly be observed around 30 T. Eventually above 10 K, the transition becomes broad and hardly identified. These results can be summarized visually as a  $H$ - $T$  phase diagram in the inset of Fig. 1.

In summary, we found for the first time a  $1/2$  magnetization plateau in the  $S=3/2$  Heisenberg pyrochlore antiferromagnet  $\text{CdCr}_2\text{O}_4$ . This spin version of a 3-1 charge ordering recently found in  $\text{AlV}_2\text{O}_4$  implies that the 3-1 ordering is quite universal in the pyrochlore lattice.

#### Authors

H. Ueda<sup>a</sup>, H. A. Katori<sup>a</sup>, H. Takagi<sup>a</sup>, H. Mitamura, T. Goto<sup>a</sup>  
<sup>a</sup>RIKEN (The Institute of Physical and Chemical Research)

## Superconductivity in Lithium Under High Pressure

K. Shimizu and T. Yagi

In light elements, it is expected that superconductivity occurs at high temperature. For example, in case of hydrogen, the transition temperature above room temperature has been predicted [1], if it is compressed high enough and transformed into metallic phase. Expected transition pressure of hydrogen into metallic phase, however, is too high to achieve using current high pressure experimental techniques. At ambient condition, lithium is the lightest metal of all the elements and superconductivity at lower pressures are expected. Previous electrical resistance measurements on lithium under high-pressure and low-temperature reported a drop of resistance at around 7 K under pressure [2], which was proposed to be the onset of superconductivity. However, because of the experimental difficulty to confine lithium in a sample chamber of high pressure vessel, no confirmation was made since then. In the present study, we have made a small pit at the top of the diamond-anvil apparatus, as shown in Fig. 1, which works as a sample chamber. Because of the extreme hardness of diamond, such machining was difficult but by using a focused ultraviolet beam from pulsed KrF-excimer laser, wavelength 248 nm, we could make such a pit. Lithium was successfully confined in this pit and the electrical resistance was measured up to 48 GPa [3]. Normal metallic behavior was observed until the pressure was raised up to 30 GPa. When the pressure was

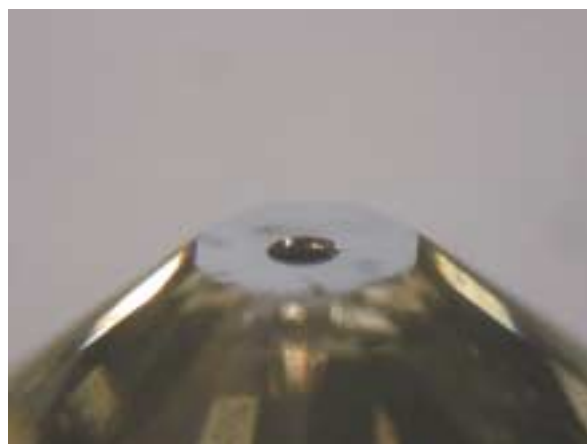


Fig. 1. A photograph of a pit prepared at the top face of diamond anvil. The size of the pit is 50  $\mu\text{m}$  in diameter and 7  $\mu\text{m}$  deep, on the 300- $\mu\text{m}$  pressure surface of the synthetic type Ib diamond anvil. The pit was prepared by a focused ultraviolet beam from pulsed KrF-excimer laser.

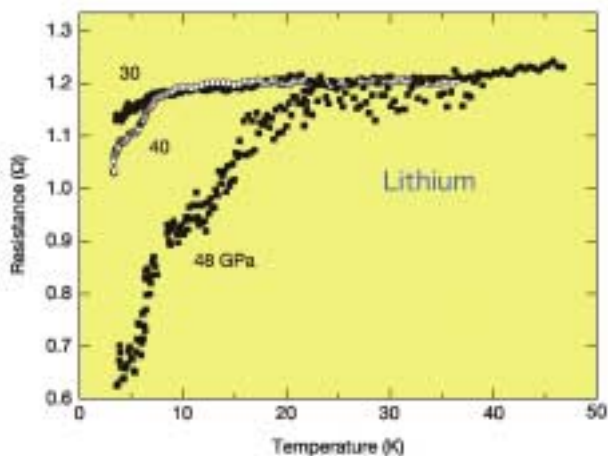


Fig. 2. Some examples of the electrical resistance of lithium measured at temperatures below 50 K. In this series of experiment, the pressure was changed at 4 K and the increment of the resistance during compression was negligible. The observed onset temperature of the drop shifted to higher temperature with increasing pressure, and reached to 20 K at 48 GPa.

increased further above 30 GPa, a drop of resistance was observed at around 7 K, as shown in Fig. 2, and the onset temperature of the drop sifted to higher temperature with increasing pressure. It has reached to 20 K at 48 GPa. The effect of magnetic fields on the behavior of the resistance drop was also measured, from which we could conclude that this drop of resistance is due to the onset of superconductivity of lithium.

In this study we showed that lithium becomes superconducting at pressures greater than 30 GPa, with a pressure dependent transition temperature ( $T_c$ ) of 20 K at 48 GPa. This is the highest observed  $T_c$  of any element; it confirms the expectation that elements with low atomic numbers will have high transition temperatures, and suggests that metallic hydrogen will have a very high  $T_c$ . According to theoretical predictions on lithium, we may be able to achieve a  $T_c$  higher than 20 K on further compression and further studies are now in progress.

#### References

- [1] C.F. Richardson and N.W. Ashcroft, Phys. Rev. Lett. **78**, 118 (1997).
- [2] T. H. Lin and K.J. Dunn, Phys. Rev. B**33**, 807 (1986).
- [3] K. Shimizu, H. Ishikawa, D. Takao, T. Yagi, and K. Amaya, Nature, **419**, 597(2002).

#### Authors

K. Shimizu<sup>a</sup>, H. Ishikawa<sup>a</sup>, D. Takao<sup>a</sup>, T. Yagi, and K. Amaya<sup>a</sup>  
<sup>a</sup>Osaka University

## Unusual Pressure Effects on CDW and Superconductivity in ZrTe<sub>3</sub>

K. Yamaya and Y. Uwatoko

In low-dimensional electron systems, there exist a variety of ground states such as charge-density-wave, spin-density-wave (CDW, SDW), and superconductivity. On investigating their coexistence or competition between them, the application of pressure has been used as a powerful tool. Pressure-induced suppression of C(S)DW and enhancement of superconductivity are understood basically by change in a nesting effect of the Fermi surface under pressure. ZrTe<sub>3</sub> is one of transition-metal trichalcogenides MX<sub>3</sub> that is well

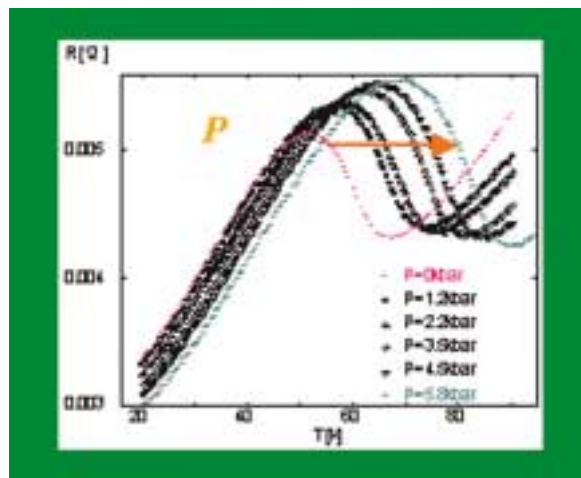


Fig. 1. Temperature dependence of resistance measured along the  $a$ -axis under pressure in ZrTe<sub>3</sub>. A humped resistance anomaly is due to the CDW transition.

known as linear chain compounds and it undergoes a CDW state near 63 K and a superconducting state at *ca.* 2 K [1]. However, the properties of CDW and superconductivity of ZrTe<sub>3</sub> are largely different from those of typical MX<sub>3</sub> such as NbSe<sub>3</sub> and TaS<sub>3</sub>; the CDW nesting vector has no component of the chain-axis direction and the superconductivity is not of bulk nature but filamentary. These features of ZrTe<sub>3</sub> lead us to an interest whether competition between the superconductivity and the CDW is explained by the Fermi surface nesting. We investigated the pressure effect of CDW and superconductivity in ZrTe<sub>3</sub> by measuring the electrical resistance down to 1.2 K under pressures up 0.6 Gpa using a clamp type piston-cylinder.

Fig. 1 shows the temperature dependence of the resistance along the  $a$ -axis between 20 K and 90 K under pressure [2]. At ambient pressure the resistance exhibits a humped anomaly near  $T_{CDW}=63$  K. As pressure increases,  $T_{CDW}$  and a magnitude of the resistance anomaly increase largely. This shows that CDW of ZrTe<sub>3</sub> is significantly enhanced under pressure.

Fig. 2 shows the temperature dependence of resistance near the superconducting transition under pressure. The transition width is broad because of the filamentary nature of superconductivity. We defined  $T_c$  as the temperature corresponding to the zero resistance.  $T_c$  decreases significantly

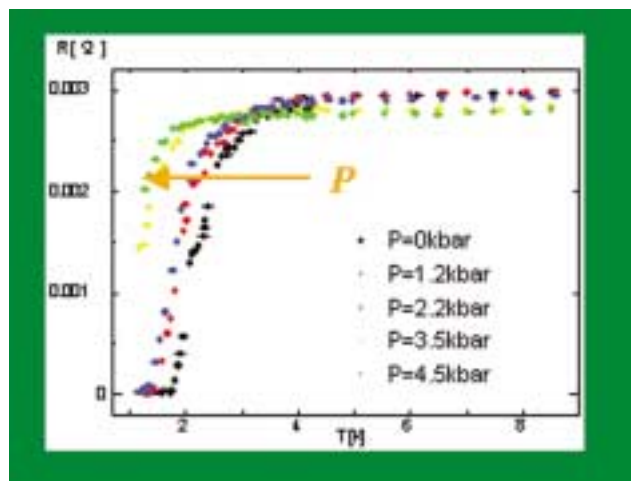


Fig. 2. Temperature dependence of resistance measured along the  $a$ -axis below 9 K under pressure. The superconducting transition width is broad, which can be represented well as the one-dimensional fluctuation even under pressure [3].

with increasing pressure, showing the strong suppression of the superconductivity under pressure [3].

Contrary to the usual pressure effect on competition between CDW and superconductivity, we found pressure-induced enhancement of CDW and suppression of superconductivity in ZrTe<sub>3</sub>. This suggests that competition between the superconductivity and the CDW is not simply explained by the nesting effect of the Fermi surface, but other origin is needed. Recent experiment of photoemission spectroscopy shows the CDW pseudogap formation growing from ~280 K [4]. The relationship between the pressure-enhanced CDW and the CDW pseudogap formation is expected, although yet inexplicable. Measurements under higher pressure are needed.

#### References

- [1] S. Takahashi, T. Sambongi and S. Okada, *J. de Phys.*, **44**, C3-1733 (1983).
- [2] K. Yamaya, M. Yoneda, S. Yasuzuka, Y. Okajima, and S. Tanda, *J. Phys.: Condens. Matter*, **14**, 10767 (2002).
- [3] K. Igarashi, S. Yasuzuka, K. Inagaki, S. Tanda, Y. Okajima, M. Hedo, Y. Uwatoko, and K. Yamaya, *J. de Phys. IV*, **12**, 97 (2002).
- [4] T. Yokoya (private communication).

#### Authors

M. Yoneta<sup>a</sup>, S. Yasuzuka<sup>a</sup>, K. Igarashi<sup>a</sup>, Y. Okajima<sup>b</sup>, K. Inagaki<sup>a</sup>, S. Tanda<sup>a</sup>, N. Hedo, Y. Uwatoko and K. Yamaya<sup>a</sup>

<sup>a</sup>Dept. Appl. Phys. Hokkaido University

<sup>b</sup>Asahikawa National College of Technology.

## Superconductivity at 14.2K in Layered Organic Under Extremely High Pressure

H. Taniguchi, M. Hedo, Y. Uwatoko

Since the pressure, in general, weakens the electron correlation, even stiffly localized electrons in the Mott insulator are expected to itinerate eventually under high pressure. Upon this concept, we have picked up the molecular-based Mott insulator,  $\beta'$ -(BEDT-TTF)<sub>2</sub>ICl<sub>2</sub> [1], among many organic systems and tried to metallize it by application of pressure, motivated by the fact that novel superconductivity was often behind the insulating phase. Because the insulating nature of  $\beta'$ -(BEDT-TTF)<sub>2</sub>ICl<sub>2</sub> is very strong, the pressure range of 0-2 GPa, which can be achieved by the widely-used piston-cylinder-type pressure cell, is not sufficient for the present requirement. Then we adopt the cubic anvil press [1], which makes it possible to measure the resistivity under high pressure in the range of 2.0-10.0 GPa. Although there are only a few studies [2,3], on the BEDT-TTF-based complex under such extreme pressure, the resistivity of the present salt has been successfully measured up to 9.4 GPa with good reproducibility.

Figure 1 shows the logarithmic resistivity of the  $\beta'$ -(BEDT-TTF)<sub>2</sub>ICl<sub>2</sub> as a function of temperature for various pressures. The insulating behavior is gradually suppressed with increasing pressure. Around 6.5 GPa, the metallic temperature variation appears in the high-temperature range followed by the low-temperature semiconducting behavior. At almost the same time, a sharp peak shows up in the low-temperature range. This peak is rapidly suppressed by further elevated pressure with gradual increase of the peak temperature. Finally, the clear superconducting transition with vanishing resistivity emerges below the normal metallic state. Detailed characterization of the pressure-dependence of the present superconductivity confirms that  $T_c$  reaches a

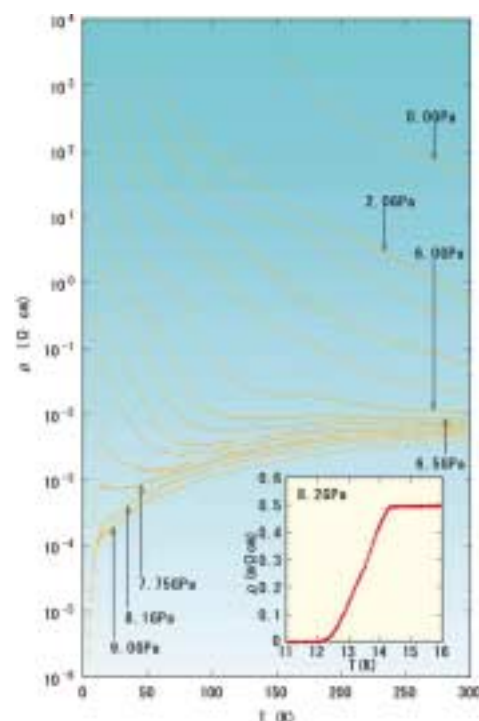


Fig. 1. Resistivity of  $\beta'$ -(BEDT-TTF)<sub>2</sub>ICl<sub>2</sub> salt as functions of temperature and pressure.

maximum value, 14.2 K (onset), at 8.2 GPa (the inset). This is the highest  $T_c$  among the organics known to date.

We have constructed the pressure-temperature phase diagram of  $\beta'$ -(BEDT-TTF)<sub>2</sub>ICl<sub>2</sub> salt through this study, as shown in the Fig.2. The superconducting phase (S) just borders on the insulating phase (I). This feature suggests that the appearance of the present superconductivity originates from unconventional mechanism, as is the case with other highly correlated electron systems. Further researches are required to clarify this issue.

#### References

- [1] N. Mori *et al.*, *JJAP Series No. 8*, p. 182.
- [2] K. Murata *et al.*, *Synth. Met.* **103**, 1891(1999).
- [3] M. Miyashita *et al.*, *Physica C* in press.

#### Principle Publication and Authors

H. Taniguchi<sup>a</sup>, M. Miyashita<sup>a</sup>, K. Uchiyama<sup>a</sup>, K. Sotoh<sup>a</sup>, N. Mori<sup>a</sup>, H. Okamoto<sup>b</sup>, K. Miyagawa<sup>c</sup>, K. Kanoda<sup>c</sup>, M. Hedo and Y. Uwatoko, *J. Phys. Soc. Jpn.* **72**, 468 (2003).

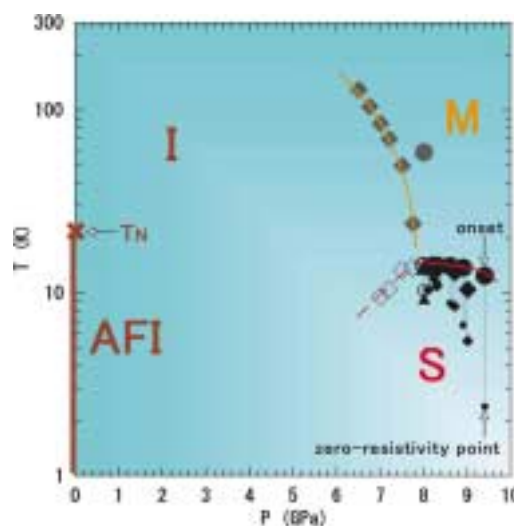


Fig.2. Pressure-temperature phase diagram of  $\beta'$ -(BEDT-TTF)<sub>2</sub>ICl<sub>2</sub>. Metallic (M), insulating (I), and superconducting (S) phases are shown.  $T_N$  of antiferromagnetic ordering has been determined only for ambient pressure.

## Novel Antiferromagnetism in Mixed Valence System $\text{YbMn}_2\text{Ge}_2$

T. Fujiwara and Y. Uwatoko

The ternary intermetallic compounds  $\text{RMn}_2\text{Ge}_2$  crystallize in the tetragonal  $\text{ThCr}_2\text{Si}_2$  type structure and their magnetic characteristics are dominated by the Mn  $3d$ –Mn  $3d$  magnetic interactions.  $\text{YbMn}_2\text{Ge}_2$  with unstable  $4f$  electron states shows a quite unique antiferromagnetism. As is shown in a  $P$ – $T$  phase diagram (Fig.1), the Néel temperatures,  $T_{N1}$  and  $T_{N2}$ , simultaneously exhibit a minimum and maximum at  $\sim 1.25$  GPa, respectively [1]. This indicates that a magnetic structural change occurs at  $P_c \sim 1.25$  GPa and AFM I state competes with AFM II state in  $\text{YbMn}_2\text{Ge}_2$ . Such a competition behavior has not been found in other  $\text{RMn}_2\text{Ge}_2$  compounds being in static  $\text{R}^{3+}$  ionic states so far. These suggest that there is a strong correlation between the valence instability of the Yb ion and the Mn  $3d$ –Mn  $3d$  magnetic interactions. Thus, we investigated a pressure dependence of a valence of Yb ionic state by X-ray absorption spectroscopy (XAS) measurements.

Figure 2 shows the normalized XAS spectra near the Yb  $L_{III}$  threshold of  $\text{YbMn}_2\text{Ge}_2$  under various pressures at 300 K. In the spectra at 0 and 0.59 GPa, we can recognize an apparent dual peaked edge structure which is typical feature in mixed valence systems. With applying pressure, the  $L_{III}$  edge spectra of this system drastically change, indicating that the mean valence of Yb ion relatively varies toward the trivalent state. These spectra can be interpreted as the superposition of two  $L_{III}$  white lines. We can obtain the fractional occupation of  $4f$  configurations from the intensity ratio of the two  $L_{III}$  white lines. In order to estimate the Yb mean valence, all the normalized spectra were analyzed in the standard procedure by fitting with two subspectra which are attributed to the  $\text{Yb}^{2+}$  and  $\text{Yb}^{3+}$  final states with the electronic configurations of  $(2p^5 4f^{14} 5d^*)$  and  $(2p^5 4f^{13} 5d^*)$ , respectively, where each subspectrum consists of a Lorentzian and an arctangent function [2]. Consequently, the Yb mean

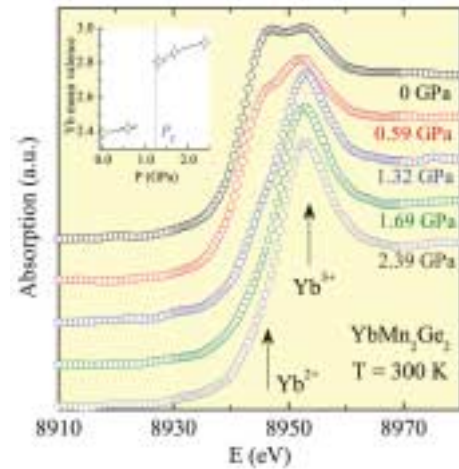


Fig. 2. X-ray absorption spectra near the Yb  $L_{III}$  threshold at 300 K under various pressures in  $\text{YbMn}_2\text{Ge}_2$ . The estimated Yb mean valence is plotted as a function of pressure in the inset

valence at ambient pressure was estimated to be  $\sim 2.4$ . This indicates that  $\text{YbMn}_2\text{Ge}_2$  is a typical mixed valence system. The estimated Yb mean valence is plotted as a function of pressure in an inset of Fig. 2. Here, the solid lines are guide to the eye for a variation of the Yb mean valence upon pressurization and the bluish broken line represents the critical pressure  $P_c \sim 1.25$  GPa which was estimated from the magnetization measurements under high pressures. It can be clearly seen that the Yb mean valence abruptly changes around  $0.9 \sim 1.25$  GPa. Therefore, we can conclude that the pressure induced phase transition at  $P_c \sim 1.25$  GPa originates in the abrupt change of Yb valence near the  $P_c$ . These results are direct evidence that the instability of Yb  $4f$  electrons state much affect on the Mn  $3d$ –Mn  $3d$  dominant interactions in  $\text{RMn}_2\text{Ge}_2$  compounds as shown in Fig.1.

### References

- [1] T. Fujiwara, H. Fujii, Y. Uwatoko, K. Koyama, M. Motokawa and T. Shigeoka, Acta Physica Pol B. **34**, 1541 (2003).
- [2] L. M. Falicov, W. Hanke and M. B. Maple. (Eds.), Valence fluctuations in Solids, North-Holland, Amsterdam, 1981.

### Authors

T. Fujiwara<sup>a</sup>, H. Fujii<sup>a</sup> and Y. Uwatoko

<sup>a</sup>Faculty of Integrated Arts and Sciences, Hiroshima University.

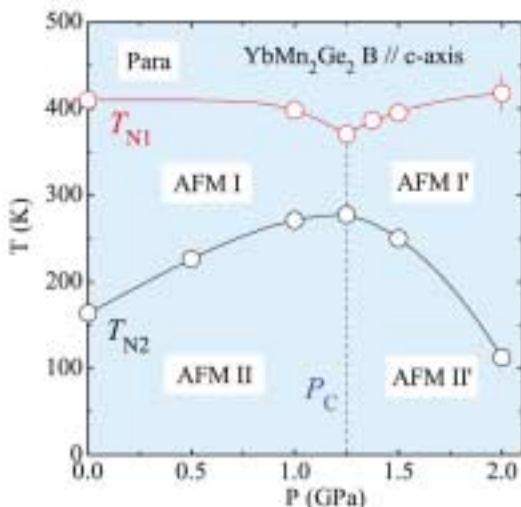


Fig. 1.  $P$ – $T$  phase diagram of  $\text{YbMn}_2\text{Ge}_2$ .

## Vortex and Texture in Rotating Superfluid $^3\text{He}$

O. Ishikawa, T. Mizusaki and M. Kubota

Texture is one of the crucial subjects in studying superfluid  $^3\text{He}$ . The texture is the configuration of internal freedom of condensation in spin space and in momentum space, where the  $\mathbf{d}$ -vector and  $\mathbf{l}$ -vector are the order parameters representing such freedom, respectively. The configuration of vectors are determined by several external conditions such as magnetic field, boundary, flow field etc.. The energy corresponding to such a condition and the internal dipole energy compete each other and make a textural pattern in the two vector fields. Sometimes texture includes a defect in the condensation state as a result of competition.

Recently three types of texture were found in narrow cylinders with  $100 \mu\text{m}$  radius in A phase. Nuclear Magnetic Resonance (NMR) technique is employed to identify each

type of texture and it became evident that rotation of the cryostat which holds the sample cylinders is an important external condition to do so, especially up to the world fastest speed of 6.28 rad/sec at a constant temperature during the whole measurement[2].

The radius of a long and narrow cylindrical sample was about ten times larger than the dipole coherence length so any suppression of the order parameter is not expected. But the boundary restriction on  $l$ -vector field strongly produces an effect on the overall texture in the cell, which is definitely different from that of bulk liquid.

Figure 1 shows three NMR absorption spectra corresponding to three types of texture, observed at  $T/T_c=0.75$  right after it was cooled through  $T_c$  from normal phase and at  $\Omega=0$  rad/sec, where  $\Omega$  is the angular velocity of the rotating cryostat. Both A and B types of texture were observed when the liquid was cooled slowly through  $T_c$  from normal phase by cooling rate of 1  $\mu$ K/min. The difference between A and B is due to the external condition of the magnetic field and the rotational direction while going through  $T_c$ . Type A texture is found under the rotation at  $\Omega=+2$  rad/sec and the magnetic field  $H=-22$ mT. On the other hand, type B texture is formed under the same rotation but the opposite magnetic field ( $\Omega=+2$  rad/sec,  $H=+22$  mT). Type C texture was observed when the liquid was cooled as fast as 10  $\mu$ K/min, ten times faster than for type A and B. This type C texture did not depend on the external condition of the magnetic field and the rotation through  $T_c$ . The creation mechanism of type C is not clear. The large intensity of satellite peak denoted by arrow may be due to the defect in texture along the sample axis.

The absorption spectra for type A and B are changed by rotating the cryostat, showing the appearance and disappearance of the satellite signal and the change of main peak over the critical angular velocity  $\Omega_n$  and under another one  $\Omega_a$ , respectively. Such a hysteresis is attributed to the quantum vortex in the cell. Assuming a single vortex in the sample liquid, the quantum number of circulation is just 3. This integer is representing a macroscopic quantum phenomena but 3 is a curious number, because the continuous vortex in A phase has the quantum number of 2. Between  $\pm\Omega_n$  the intensity of main peak changed a little by rotation. This means that each type A and B texture has an angular momentum to couple with the rotation even in this rotating speed. But it is evident to any one that the behavior of type A and B is very different from each other (Fig.2). So the

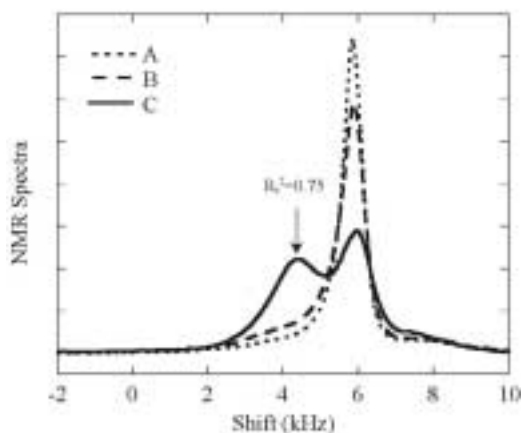


Fig. 1. NMR absorption spectra for  $\Omega=0$  at  $T/T_c=0.75$  as a function of frequency shift from the Larmor frequency. Spectra for 3 textures labeled by a dotted line for A, a dashed line for B and a solid line C are shown.

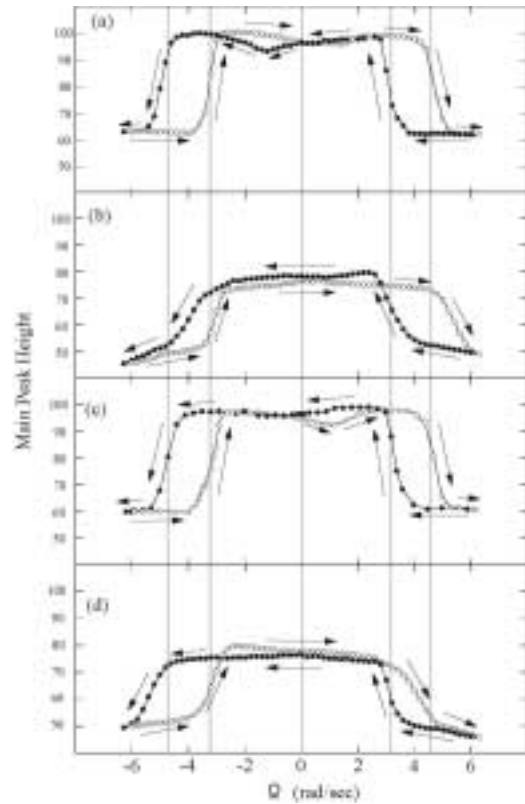


Fig. 2. NMR absorption of the main peak as a function of rotation speed  $\Omega$  during acceleration and deceleration cycle. The condition of cooling the sample through  $T_c$  are : (a) (+2 rad/sec, -22 mT), (b) (+2 rad/sec, +22 mT), (c) (-2 rad/sec, +22 mT), (d) (-2 rad/sec, -22 mT). The spectra (a) and (c) corresponds to type A texture and (b) and (d) to type B. Arrows indicate the direction of taking data and vertical lines are  $\Omega_n$  and  $\Omega_a$  for type A.

types A and B texture have different configurations of  $l$ -vector possessing the same angular momentum which may explain the same critical angular velocity  $\Omega_a$  for vortex disappearance in both types of texture.

We believe that we are starting up a new field of superfluidity study where variety of internal freedom of Cooper pairs plays interesting new phenomena.

#### References

- [1] R. Ishiguro, M.Yamashita, O.Ishikawa, *et al.*, Physica B329-333, 66(2003).
- [2] M. Kubota, *et al.*, Physica B329-333, Part1 1577(2003).

#### Authors

O. Ishikawaa and M. Kubota.  
aOsaka City University

## ISSP WorkShop (April 2002 ~ March 2003)

### 1. Frustrated magnetism and novel properties

June 19 ~ 21, 2002

Frustration is ubiquitous in nature. It describes the situation where several optimization conditions compete with each other and are incompatible. Under frustration, the system tends to be unstable and is often subject to strong fluctuation effects, which could give rise to many interesting novel phenomena not encountered in standard unfrustrated systems. In the ISSP workshop, we concentrated on frustrated magnetism and related novel phenomena in condensed matter physics. The topics covered were fairly wide, from the nature of various novel magnetic phase transitions and ordered states of frustrated magnets, to novel transport and electronic properties of metallic frustrated systems. Mentioning some of the topics hotly discussed, magnetic ordering of kagome and pyrochlore magnets including spin ice, quantum spin ordering of geometrically frustrated magnets, nature of the ordering of chirality and its effect on transport properties such as anomalous Hall effect, geometrical frustration and strongly correlated electron systems, ordering and off-equilibrium dynamics of spin glasses, etc.

### 2. New developments in glass physics

July 10 ~ 12, 2002

The glass forming process is a transition from liquids to solids in non-equilibrium systems and is a phenomenon totally different from crystallization. Recent extensive studies in Japan and around the world have revealed that the dynamical and thermodynamic characteristics of the glass forming process could be understood in a unifying manner on the basis of the energy landscape picture. In this workshop, latest results from experimental, theoretical and computational studies were presented with emphasis on the glass transition and the properties of glasses. From the intensive discussions following each oral presentation and in the poster session, a new direction of the research on glass physics has emerged, which will be pursued as some joint efforts.

### 3. High field science-present status and perspectives

October 8 ~ 9, 2002

The purpose of this workshop is to establish near future perspectives on high field science in Japan, especially in the field of condensed matter physics. For this purpose, selected reviewers are invited to give overviews on important fields of high field science. Topics included are superconductivity, semiconductor physics, quantum spin systems, material processing, chemistry and various types of spectroscopy in high magnetic fields. In addition, several novel topics on researches in high magnetic fields are shown. Examples of topics are THz spectroscopy, quantum plateau, quantum phase transition and novel strongly correlated systems in high magnetic fields. The present status of major high field facilities and independent high field laboratories are also reported. The final session is devoted for the establishment of High Magnetic Field Forum of Japan. The first meeting of the forum is successfully made and the organizing committee is selected (for details, see <http://www.issp.u-tokyo.ac.jp/contents/others/himag-forum/index.html>).

### 4. Physics of friction

October 23 ~ 25, 2002

Friction is one of the most familiar physical phenomena and its research has long history due to its importance. The fundamental mechanism of friction is, however, not well understood still now. Recently many new experimental techniques, such as surface controlling technique, Ultra High Vacuum technique, Atomic Force Microscope, Frictional Force Microscope, Quartz Crystal Microbalance technique, Surface Force Apparatus and so on, enable us to investigate frictional phenomena from a modern point of view along with the progress of theoretical and numerical studies. The physics of sliding friction at solid surface has strong relation with many problems in conventional condensed matter physics, i.e., vortex and density wave dynamics, etc. In this workshop we had about 50 talks and discussed lively recent progress of "physics of friction" in various systems for 3 days.

### 5. Computational physics in condensed matter research

November 6 ~ 8, 2002

Recent developments of the field, achieved mostly by making use of the supercomputer system in the Supercomputer Center at ISSP, were discussed in the workshop. Particularly emphasized were new computational methods which, combined with large-scale calculations, enable us to analyze various cooperative phenomena in condensed matters. They are time-dependent density functional molecular dynamics simulations, first-principles approaches for strongly correlated systems and for transition-metal surfaces, the path integral renormalization group method, the non-equilibrium relaxation method, the probability-changing cluster algorithm, and so on. In a special session of the workshop, we also discussed the present status of, and future requirements for the ISSP supercomputer system, which is placed at the service of general researchers of condensed matter physics in Japan.

## 6. New materials and new functions in molecular conductors

November 25 ~ 27, 2002

Cooperation of chemistry and physics has been an important impetus in the research field of molecular conductors. Recently, record high  $T_c$  of organic superconductors has been raised to 14.2 K by the application of extremely high pressure. Superconductivity is realized in newly designed donor molecules, which include novel superconductors with enhanced electron correlation and those with incommensurate structures. In addition, new materials have developed characteristic new physics; examples are structure-property correlation such as the universal phase diagram, charge order, large uniaxial strain effects, and field-induced superconductivity and giant magnetoresistance in  $\pi$ d-systems. Recent ideas coming from device physics and nano science are also giving large impacts on this field. In this workshop, specialists in this research field, together with researchers who are interested in molecular conductors from the new point of view, provide a survey of the recent research, and discuss the development aiming at new functions.

## 7. Materials researches in the 21 century using new-generation VUX / SX light sources

December 13 ~ 14, 2002

In relation to the new VUV / SX light source project supported by all users, recent hot results and new research possibilities using synchrotron radiation in solid-state science and technology were presented by actively working young researchers. The workshop attracted over 90 scientists from universities, national institutes and private companies. The workshop covered wide variety of spectroscopic studies on nanostructures, magnetic ultrathin films, superconducting materials, organic-device related materials, surface dynamics, and surface chemistry. Topics of new experimental techniques and instrumentations related to these studies were also included. In addition to these, a promising idea to obtain ultrashort synchrotron-radiation pulse was introduced by accelerator group. Very exciting discussions were made throughout the workshop. Discussions clearly indicated that spectromicroscopy, photoelectron emission microscopy (PEEM), time-resolved spectroscopy and very high-resolution spectroscopy coupled with the new generation VUV / SX light source with high brilliance and polarization tunability will undoubtedly open new sciences in these fields.

## 8. Manipulation and assembly of atoms and molecules based on nanomechanics

January 20 ~ 21, 2003

The atomic force microscope (AFM) is a unique microscope based on a nanomechanical method, which has the following characteristics; (1) it has true atomic resolution, (2) it can measure atomic force (so-called atomic force spectroscopy), (3) it can observe even insulators, and (4) it can measure mechanical responses such as elastic deformation. Indeed, during the last few years, the noncontact AFM (NC-AFM) achieved the true atomic resolution on various surfaces, the three-dimensional mapping of atomic force, discrimination of atomic force mechanisms, discrimination of atom species on sample surfaces, control of atomic force between the tip and sample atoms, control of atom position on sample surfaces, and mechanical atom manipulation. In this workshop, recent activities on atoms, molecules and biopolymers based on the nanomechanical method are reported and we discussed how to approach to manipulate and then assemble atoms and molecules into nanostructures both experimentally and theoretically.

## 9. Present and future of research in high magnetic fields

May 29, 2002

The use of high magnetic fields for material research is rapidly developing nationally and internationally in these days as the magnet technology becomes advanced. In the United States and Europe, large-scale facilities to generate high magnetic fields are being built one after another under government projects. Considering such situation, we need immediately to make closer cooperative relationship among research groups in Japan in order to strengthen our research system and create outstanding results which can lead the world of high magnetic field again. Therefore, magnetic field researchers in Japan agreed to establish "The High Magnetic Field Forum of Japan" to promote study of high magnetic field physics in Japan. In the process of discussing the forum, we found that it might be necessary to construct a long pulse magnet facility as a facility for professional joint research. In this workshop, leading people in various fields of solid state physics made their own proposals for the possibility of science that a new facility enables us to pursuit for the first time.

## **10. DSC workshop**

June 12 ~ 13, 2002

The Materials Design and Characterization Laboratory (MDCL) in ISSP aims to promote materials science with an emphasis on the "DSC cycle" where DSC is integration of three functions, Design, Synthesis and Characterization. Recent activities on various topics of materials development, including the results obtained by User Programs, were presented as 28 talks and discussed in this workshop. A new direction of the research and a future plan of MDCL were also discussed. The workshop was very successful with active discussions among more than 50 participants.

## **11. Research prospects on atom- and molecular- spectroscopy and biology using VUX / SX high-brilliant light source**

September 17 ~ 18, 2002

In relation to the new VUV / SX light source (Super SOR) project, recent hot results and new prospects using synchrotron radiation in atom- and molecular spectroscopy and biology were presented by actively working young researchers. The workshop attracted 37 scientists from universities, national institutes and private companies. The workshop covered spectroscopic studies of atoms, molecules and clusters, soft-X-ray imaging, and radiation effect to bio-matters. The status of the project as well as the design of the beamline monochromators were also introduced. Most of the proposals were challenging and interesting. Especially, the new optical mount for the soft-X-ray emission spectroscopy monochromator by Dr. Hatsui (IMS) was very impressive. It was noticed further that the demands to the micro-beam or imaging techniques using Super SOR is very high.

## **12. Future plan on neutron scattering sciences in soft matter physics**

October 25 ~ 26, 2002

Neutron scattering technique has been one of the most powerful tools for nanostructure investigations as well as molecular dynamics studies on soft matter physics. The year of 2001 was the last of a ten-year contract of the Neutron Scattering Laboratory, ISSP, and for renewal starting from 2002. On this occasion, a workshop on future directions of soft matter physics with neutron scattering techniques was held on Oct. 25 and 26, 2002, at Neutron Scattering Laboratory, Tokai. More than 40 participants attended and discussed on various themes, including (1) today and future of neutron sources and the guide hall of JRR-3M, (2) refurbishment and/or construction of the neutron spectrometers, (3) the relationship between the J-PARC Plan and JRR-3M, and (4) soft matter science and the amenity and laboratory environments at Tokai. It was recognized that neutron scattering techniques would become more fundamental and key tools for soft matter science. Hence, further financial and personnel support from the government and funding organizations would be strongly recommended.

## **13. Dr. Rohrer's JSPS award workshop III and ISSP international workshop — a role of physics for nano science and technology —**

February 17 ~ 18, 2003

Dr. Heinrich Rohrer, a Nobel laureate in Physics for an invention of scanning tunneling microscopy, was awarded by Japan Society for the Promotion of Science (JSPS) as a Prominent Scientist. Commemorating the award-winning, a workshop has been held every half year with Dr. Rohrer as a honorary participant. This workshop, combined with an ISSP international workshop, is the third one of the JSPS workshop series. Main theme of this workshop is nano science and technology, which Dr. Rohrer pioneered, and their physics sides was particularly discussed. Presented subjects included molecular excitation and manipulation, controlled cluster formation, nanotube technology, functional one-dimensional structure, novel techniques for high-resolution AFM and ultrafast STM, Coulomb blockade and coherence, and etc. With 14 talks including 2 invited talks from abroad, 34 posters and more than 100 participants, the discussion at the workshop was very active and fruitful.